Article

Cell Reports

Physcomitrium patens PpRIC, an ancestral CRIB-domain ROP effector, inhibits auxin-induced differentiation of apical initial cells

Graphical abstract

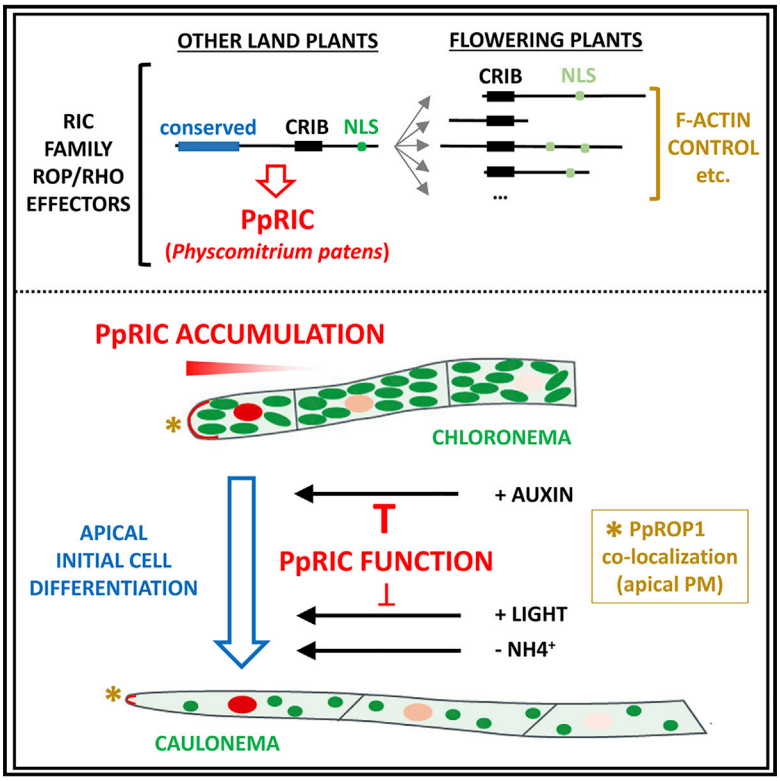

Highlights

- The PpROP interactor PpRIC is the only homolog of key RHO effectors in *P. patens*
- PpRIC homologs are structurally conserved in most land plants except flowering plants
- PpRIC has nuclear functions, while most flowering plant homologs modulate F-actin
- PpRIC specifically blocks auxin- and high-light-induced caulonema differentiation

Authors

Maria Ntefidou, D. Magnus Eklund, Aude Le Bail, ..., Anna Bannmüller, Karin Ljung, Benedikt Kost

Correspondence

benedikt.kost@fau.de

In brief

Ntefidou et al. show that RICs, key CRIB-domain effectors of ROP (RHO of plant) GTPases, are represented by few closely related homologs in most land plants but display massive diversification in flowering plants. Whereas most flowering plant RICs modulate cytoplasmic F-actin, moss PpRIC has nuclear functions in maintaining apical initial cell identity.

Ntefidou et al., 2023, Cell Reports *42*, 112130
February 28, 2023
https://doi.org/10.1016/j.celrep.2023.112130

CellPress

Cell Reports

CellPress
OPEN ACCESS

Article

Physcomitrium patens PpRIC, an ancestral CRIB-domain ROP effector, inhibits auxin-induced differentiation of apical initial cells

Maria Ntefidou,[1,4] D. Magnus Eklund,[2,4] Aude Le Bail,[1,4] Sylwia Schulmeister,[1] Franziska Scherbel,[1] Lisa Brandl,[1] Wolfgang Dörfler,[1] Chantal Eichstädt,[1] Anna Bannmüller,[1] Karin Ljung,[3] and Benedikt Kost[1,5,*]

[1]Cell Biology, Department of Biology, University Erlangen-Nuremberg, 91058 Erlangen, Germany
[2]Physiology and Environmental Toxicology, Department of Organismal Biology, Uppsala University, 75236 Uppsala, Sweden
[3]Umeå Plant Science Centre, Department of Forest Genetics and Plant Physiology, Swedish University of Agricultural Sciences, 90183 Umeå, Sweden
[4]These authors contributed equally
[5]Lead contact
*Correspondence: benedikt.kost@fau.de
https://doi.org/10.1016/j.celrep.2023.112130

SUMMARY

RHO guanosine triphosphatases are important eukaryotic regulators of cell differentiation and behavior. Plant ROP (RHO of plant) family members activate specific, incompletely characterized downstream signaling. The structurally simple land plant *Physcomitrium patens* is missing homologs of key animal and flowering plant RHO effectors but contains a single CRIB (CDC42/RAC interactive binding)-domain-containing RIC (ROP-interacting CRIB-containing) protein (PpRIC). Protonemal *P. patens* filaments elongate based on regular division and PpROP-dependent tip growth of apical initial cells, which upon stimulation by the hormone auxin differentiate caulonemal characteristics. PpRIC interacts with active PpROP1, co-localizes with this protein at the plasma membrane at the tip of apical initial cells, and accumulates in the nucleus. Remarkably, PpRIC is not required for tip growth but is targeted to the nucleus to block caulonema differentiation downstream of auxin-controlled gene expression. These observations establish functions of PpRIC in mediating crosstalk between ROP and auxin signaling, which contributes to the maintenance of apical initial cell identity.

INTRODUCTION

Animal and plant RHO guanosine triphosphatases (GTPases) are important regulators of cell differentiation and behavior during normal development and defense responses.[1,2] The signaling activity of most RHO GTPases depends on post-translational lipid modifications responsible for plasma membrane association and is controlled by largely conserved upstream regulation.[3] RHO GTPases typically interact with multiple downstream effectors to coordinate different cellular processes including F-actin reorganization, membrane trafficking, and gene expression.[4] Although some RHO effectors such as NOXs (NADPH oxidases) and PI4P5Ks (phosphatidylinositol 4-phosphate-5-kinases) appear to have conserved functions in all eukaryotes, activated RHO GTPases stimulate strikingly different downstream signaling in animals and plants.[5,6] Key effectors of animal RHO GTPases are missing in plants, including PAK (P21-activated kinases) and ROCK (RHO-associated kinase) family protein kinases, which specifically interact with activated RHO GTPases via a CRIB (CDC42/RAC interactive binding) domain.[5] Instead, plant-specific ROP (RHO of plant) GTPase effectors such as RIC (ROP-interacting CRIB-containing[7]), ICR/RIP (interactor of constitutive active ROP/ROP interactive partner[8,9]), and RISAP (RAC5 interacting subapical pollen tube protein[10]) homologs have been identified. Although plant RICs contain a CRIB domain, they show little sequence similarity outside of this domain to animal PAK or ROCK kinases, or to other known proteins.[11]

An important and well-characterized function of plant ROP GTPases is the control of directional cell expansion.[12,13] ROPs specifically associate with the plasma membrane at the tip of lobes extending from developing leaf epidermal cells as well as at the apex of cells expanding by unidirectional tip growth, such as pollen tubes and roots hairs. *Arabidopsis thaliana* and other flowering plants (angiosperms) contain large families of structurally diverse RICs,[7] which in response to ROP activation play central roles in the regulation of polar cell expansion together with other effectors.[14,15] Different RICs with distinct functions in the modulation of cytoskeletal organization are required for this process.[16] In flowering plants, RICs are also essential mediators of ROP-controlled stomatal opening,[17,18] long-distance hormone transport,[19–21] and defense responses.[22] However, the molecular mechanisms underlying RIC functions are generally not well understood.

The moss *Physcomitrium patens* is a simple non-vascular land plant, which is more closely related to green algae and to ancestral land plants than vascular plants including flowering plants.[23] The *P. patens* genome encodes four nearly identical PpROPs, but no ICR/RIP- or RISAP-related proteins and only a single PpRIC protein, which outside of the CRIB domain shares little similarity with RICs of flowering plants.[11] Hence, the functional characterization of PpRIC represents a unique opportunity to gain new insights into ROP-dependent downstream signaling and the evolution of this process.

P. patens development[24] is initiated with the germination of haploid spores, which results in the formation of branched filamentous protonemata. An apical initial cell at the tip of each protonemal filament expands unidirectionally by tip growth and regularly divides transversely, resulting in filament elongation. Young, chloronemal protonemata expand relatively slowly on the substrate surface and are rich in chloroplasts. Developmental or environmental cues trigger poorly characterized molecular and cellular mechanisms inducing gradual caulonema differentiation of apical initial cells, which results in faster tip growth, a higher proliferation rate, and the formation of oblique rather than perpendicular cell walls during transverse cell division. Caulonemal filaments also contain fewer chloroplasts and have acquired the competence to form gametophores (leafy shoots). These structures develop from lateral buds emerging from subapical caulonemal cells and form filamentous rhizoids, which grow into the substrate. Although rhizoids do not contain chloroplasts, they are otherwise structurally similar to caulonemal filaments and expand based on the same cellular mechanisms. At the tip of mature gametophores, male (antherida) and female (archegonia) reproductive organs are produced. Fertilization within archegonia results in the formation of zygotes developing into tiny diploid sporophytes, which grow on top of gametophytes and complete the live cycle by producing haploid spores.

Total loss of PpROP activity disrupts cellular polarization and restricts *P. patens* development to the formation of small clumps of irregularly shaped and arranged cells.[25–27] Different PpROPs accumulate at the plasma membrane at the tip of apical protonemal initial cells, where they promote tip growth like their homologs in flowering plants.[25–28] PpROPs may also contribute to the spatial control of filament branching and apical cell division, as early during these processes they associate with the plasma membrane at sites at which lateral filaments are later emerging or where new cell walls between apical and subapical cells will be positioned.[26,27] Very little is currently known about the downstream signaling network that mediates these PpROP functions.

Caulonema differentiation of apical initial cells is controlled by the plant hormone auxin.[29–31] Enhanced auxin biosynthesis resulting from overexpression of the transcription factors PpSHI1 and PpSHI2 promotes caulonema differentiation, whereas loss of these proteins has the opposite effect.[32] Disrupting the expression of the auxin transporters PpPINA and PpPINB increases the auxin content of protonemata and also promotes caulonema differentiation. These proteins appear to mediate tip-directed auxin transport through protonemal filaments as well as excretion of this hormone from apical initial cells into the extracellular environment.[33] Via the conserved TIR-AUX/indole-3-acetic acid (IAA) pathway,[34,35] active auxin signaling induces expression of the transcription factors PpRSL1 and PpRSL2, which are essential for caulonema differentiation and strongly promote this process upon overexpression.[31] Although different environmental conditions including high light intensity and limited N_2 supply were proposed to induce caulonema differentiation,[36–38] it has not been investigated whether they do so by stimulating auxin signaling. Furthermore, no information is available about possible crosstalk in chloronemal apical initial cells between auxin-induced caulonema differentiation and PpROP-controlled tip growth, although (1) caulonema differentiation coincides with enhanced tip growth[39,40] and (2) interactions between auxin and ROP signaling have important functions in the control of cell differentiation in flowering plants.[19,41,42]

Here, an encompassing characterization of the role played by PpRIC in the elongation and differentiation of protonemal filaments is discussed in the light of an extensive comparison of algal and land plant *RIC* gene families. Data presented establish strikingly different functions of the ancestral ROP effector PpRIC as compared with previously characterized structurally distinct flowering plant homologs. In contrast to these homologs, PpRIC (1) is not essential for ROP-controlled directional cell expansion but blocks auxin-induced caulonema differentiation, and (2) is shown to require nuclear targeting for its function. Detailed analysis demonstrated that PpRIC blocks caulonema differentiation downstream of auxin-controlled gene expression but appears to display auxin-independent activity. Auxin-induced caulonema differentiation therefore seems to be attenuated by unidentified regulatory factors, which stimulate ROP signaling to activate PpRIC. Remarkably, PpRIC does not block or only incompletely blocks caulonema differentiation induced by environmental factors, indicating that this process can be stimulated by additional signaling pathways, which are at least partially auxin and ROP independent.

RESULTS

RIC proteins emerged in green algae, remained structurally conserved in most land plants, and rapidly diversified in flowering plants (angiosperms)

To characterize origin and evolution of the RIC family, different genome and transcriptome databases were searched for plant and algal RIC or ROP homologs. Databases searched, species represented in these databases, and RICs identified are listed in Table S1, which also indicates the presence of ROPs in the analyzed species. Figure 1 displays the RIC families identified in representative species of all major clades of plants (viridiplantae: land plants and green algae). A tree displaying phylogenetic relationships among the members of these RIC families is presented in Figure S1.

No RICs were identified in rhodophyte (red algae) or glaucophyte species (Table S1), which are closely related to the viridiplantae, or in chlorophytes (Figure 1), the most distant relatives of the land plants among the green algae. By contrast, genes coding for RIC-like proteins were found in some charophytes (Figure 1 and Table S1), a paraphyletic group of green algae from which the land plants originated.[43] Furthermore, structurally somewhat distinct RICs were identified in mosses, which

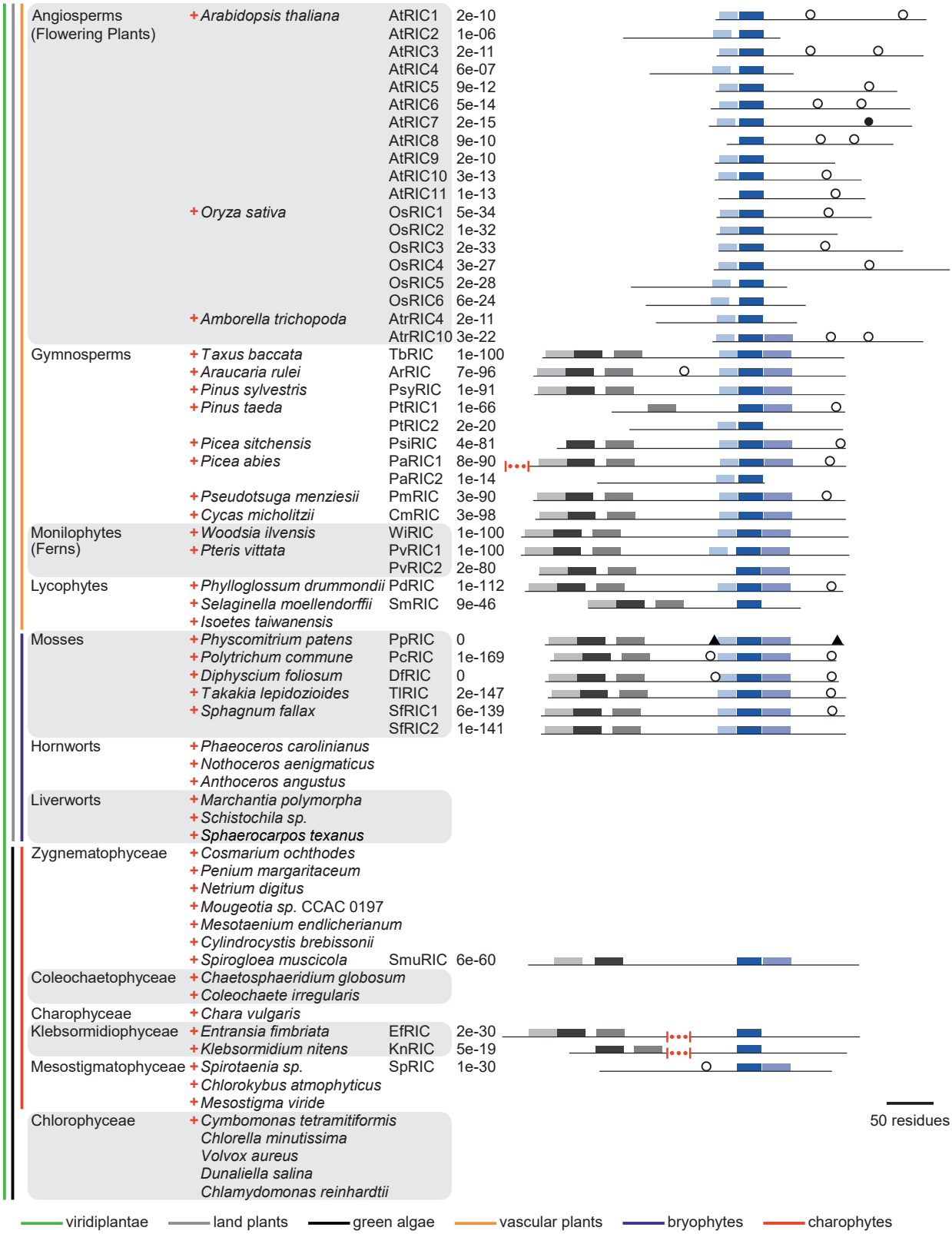

(legend on next page)

together with hornworts and liverworts form the clade of bryophytes. Among the land plants, the bryophytes are most closely related to the green algae and to ancestral land plants (Figure 1). Interestingly, 35 of 42 analyzed moss species contain one or two structurally conserved RICs, whereas no RICs were identified in 27 liverwort or 10 hornwort species (Figure 1 and Table S1).

Although the phylogenetic relationships between charophytes and land plants are unclear,[44] one of the three charophyte lineages containing RICs was proposed to represent a sister group of the land plants (Zygnematophycea), whereas the other two (Klebsormidiophyceae and Mesostigmatophyceae) appear to be more distantly related.[43] Furthermore, recent analyses of bryophyte phylogeny indicated that the hornworts split as a separate clade from a branch, which later diverged into mosses and liverworts.[45–48] This phylogenetic background and data shown in Figure 1 suggest that RICs first emerged among the charophytes and were maintained within ancestors of the land plants but were lost in some charophytes, as well as in ancestors of the hornwort and liverwort clades. An early land plant ancestor appears to have evolved a somewhat modified RIC structure, which remained highly conserved in mosses and most other land plant lineages except flowering plants. It is interesting to note that the majority of all analyzed rhodophytes (20 out of 27) and glaucophytes (1 out of 3), the green alga *Cymbomonas tetramitiformis*, as well as most investigated charophytes (40 out of 46) and bryophytes (71 out of 79) contained at least one *ROP* gene, whereas no RICs were detected in the genomes or transcriptomes of many of these species (Figure 1 and Table S1). *RIC* genes therefore have not necessarily co-emerged together with *ROP* genes.

In addition to the characteristic CRIB domain, all moss RIC proteins contain other highly conserved sequence motifs (Figure 1), some of which are already present in charophyte RICs. Three of these motifs form a conserved domain of about 105 amino acids at the N terminus of all moss RICs, which does not show sequence similarity with known proteins outside of the RIC family. In addition, one or two nuclear localization signals (NLSs) were identified at conserved positions in most moss RICs and in one charophyte homolog (Figure 1 and Table S1). RIC families were also investigated in vascular plant species (Figure 1 and Table S1). Like most mosses, a large majority of all analyzed lycophytes, monilophytes (ferns), and gymnosperms contain one to two *RIC* genes. The proteins encoded by these genes generally share high sequence and structural similarity with moss RICs and contain the same conserved sequence motifs, often along with a predicted NLS, at largely conserved positions. Interestingly the RIC family appears to have structurally evolved and rapidly expanded in flowering plants (angiosperms). Rice (*Oryza sativa*) and *Arabidopsis thaliana* contain 6 or 11 members of this family, respectively (Figures 1 and S1). All identified flowering plant *RIC* genes, including those of *Amborella trichopoda*, the basal-most flowering plant that constitutes a sister group to all other members of this clade,[49] code for proteins with relatively short N termini upstream of the CRIB domain, which are missing the N-terminal sequence motifs that are highly conserved among most other land plant RICs. Instead, flowering plant RICs appear to have evolved variable C-terminal extensions, which share little sequence similarity within the RIC family or with other known proteins. In many cases, these extensions contain one or two predicted NLSs (Figure 1). Whether these NLSs are generally functional is unclear, as only AtRIC7 was reported to be targeted to the nucleus to date,[17,18] although several other *Arabidopsis*[19–21,50–52] and barley[22] RIC proteins have also been functionally characterized. In any case, consistent with the striking structural diversification observed within the flowering plant RIC family, clearly distinct functions have been assigned to the different members of this family characterized to date.

Low-level PpRIC expression in protonemal filaments displays a tip-to-base gradient

To complement current knowledge concerning RIC functions in flowering plants, an encompassing investigation of the role played by PpRIC in the development of moss protonemata was performed. Quantitative RT-PCR (qRT-PCR) analysis demonstrated low Pp*RIC* transcript levels in protonemata and gametophores, with much higher levels detected in sporophytes (Figure 2A). In protonemata, Pp*RIC* transcripts were about 5- to 6-times less abundant than transcripts of the four Pp*ROP* genes (Figure 2B). All these observations are in agreement with published RNA-sequencing data.[28,53–55]

To further characterize the PpRIC expression pattern, reporter lines expressing a PpRIC-GUS (β-glucuronidase) fusion protein under the control of the endogenous Pp*RIC* promoter (PpRIC^{pro}) were generated. To this end, a *uidA* cDNA encoding GUS was knocked into the Pp*RIC* locus based on homologous recombination to create a genomic PpRIC^{pro}:PpRIC^{gDNA}-*GUS* reporter gene at this locus (Figures S2A and S2B). Reporter lines expressing full-length PpRIC fused to GUS at essentially endogenous levels (Figure 2C) and displaying normal development were subjected to histochemical GUS assays. Blue staining indicating PpRIC-GUS distribution was detected in protoplasts 1 day after isolation, as well as in all cells of 2-day-old protonemata regenerating from these protoplasts (Figure 2D). Interestingly, the longest chloronemal and caulonemal filaments of regenerating 5-day-old protonemata displayed a pronounced tip-to-base PpRIC-GUS distribution gradient with highest activity detected in apical and subapical cells (Figure 2D). At this stage, PpRIC-GUS was generally not detectable in short chloronemal filaments. Moderately stained long filaments frequently revealed PpRIC-GUS accumulation in the nucleus (Figure 2D, arrow). In

Figure 1. Origin and evolution of the RIC family

Domain structure of all RICs homologs of representative viridiplantae species identified in publicly available genome or transcriptome databases. Identified RIC proteins are listed after the species names (numbers: BLASTp e values). red plus sign denotes species containing at least one ROP homolog. Domain structures are drawn to scale (except for red dotted lines: motif-free 100-amino-acid fragments). Dark blue bars: CRIB domain; gray and light-blue bars: conserved motifs; black circles or triangles: predicted nuclear localization signals (NLSs); closed circle: NLS of AtRIC7, which is targeted to the nucleus as determined by fluorescent protein tagging;[17,18] closed triangles: NLSs of PpRIC, which is targeted to the nucleus depending on the identified NLSs as determined by fluorescent protein tagging and mutagenesis (this study). Scale bar represents 50 amino acid residues.

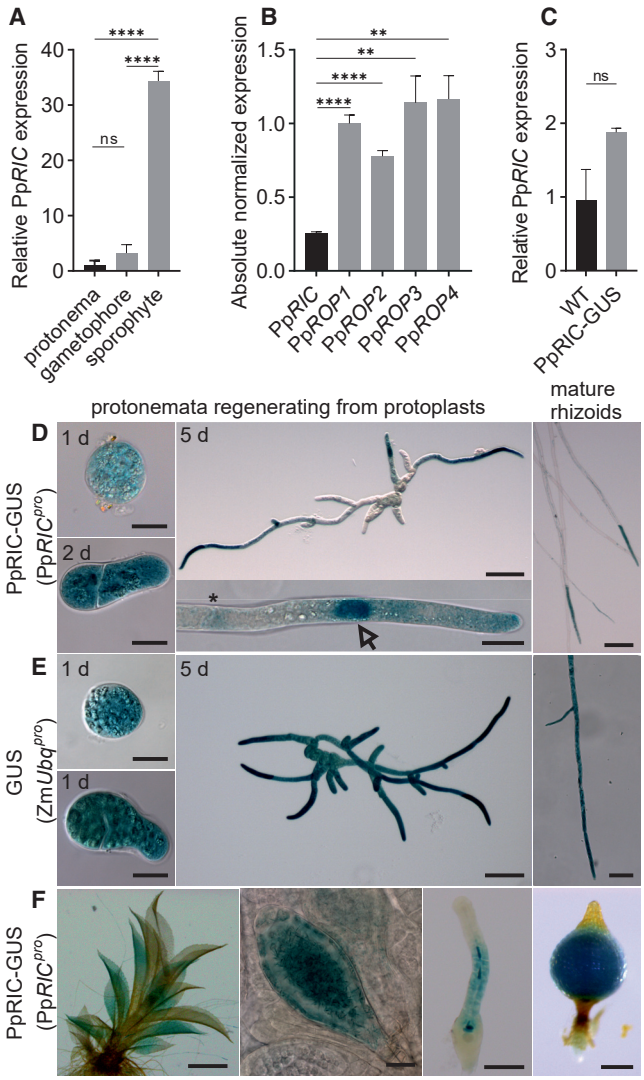

Figure 2. PpRIC expression pattern as determined by qRT-PCR and PpRIC-GUS reporter lines

(A–C) qRT-PCR analyses of Pp*RIC* transcript levels in the indicated WT moss tissues (A), in WT protonemata as compared with Pp*ROP* transcript levels (B), and in protonemata of PpRIC-GUS reporter plants (C). Relative Pp*RIC* transcript levels (A and C) or absolute transcript levels of different genes (B) are shown. Error bars denote SEM. Statistical analysis by one-way ANOVA/Tukey's test (A), one-way Welch's ANOVA (B), or unpaired Student's t test (C): ns, $p > 0.05$; **$p \leq 0.01$; ****$p \leq 0.0001$.

(D and F) Histochemical analysis of GUS activity in PpRIC-GUS reporter plants (two independent lines), expressing a PpRIC-GUS fusion protein at endogenous level (see C) under the control of the Pp*RIC* promoter (PpRIC^{pro}).

(E) Histochemical analysis of GUS activity in transgenic plants (three independent lines) expressing free GUS under the control of the *Z. mays* ubiquitin promoter (ZmUbq^{pro}).

(D and E) Protoplasts 1 day after isolation (top left; scale bar, 20 μm), regenerating protonemata 2 days (bottom left; scale bar, 20 μm) or 5 days (center; scale bar, 100 μm) after protoplast isolation, and rhizoids emerging from gametophores (right; scale bar, 100 μm). Inset in (D) (bottom center): moderately labeled apical cell of a PpRIC-GUS protonemal filament at higher magnification (scale bar, 20 μm). Arrow points to nucleus. Asterisk indicates cell wall between apical and subapical cell.

rhizoids formed by developing gametophores and in lateral branches emerging from them, PpRIC-GUS activity also displayed a tip-to-base gradient and generally appeared to be largely confined to apical cells (Figure 2D). By contrast, free GUS stably expressed under the control of the constitutively active *Zea mays* ubiquitin promoter (ZmUBQ^{pro}) showed an essentially even distribution in 5-day-old protonemal filaments and in rhizoids, with only a weak tendency to preferentially accumulate at the tips (Figure 2E). Consistent with the qRT-PCR data described above (Figure 2A), PpRIC-GUS was also detected at later developmental stages in different gametophore tissues, in reproductive organs (antheridia and archegonia), and in sporophytes (Figure 2F).

PpRIC co-localizes with PpROP1 at the plasma membrane at the tip of protonemal filaments and strongly accumulates in the nucleus

Expression of a YFP-PpROP1 fusion protein at endogenous levels in knockin lines generated by introducing a *YFP* cDNA into the genomic Pp*ROP* locus based on homologous recombination was too low to be detectable by fluorescence microscopy.[28] Estradiol-titratable expression of this fusion protein at the lowest detectable level was therefore employed to demonstrate its accumulation at the plasma membrane specifically at the tip of protonemal apical initial cells as well as along cross walls separating these cells from subapical cells (Figure 3A).[28] Association with essentially the same plasma membrane domain at the tip of apical initial cells was also reported for PpROP4 N-terminally fused to mNeonGreen or sandwich-tagged with this fluorescent protein.[26,27]

As Pp*RIC* displays substantially lower transcript levels than Pp*ROP1* (see Figure 2B), not surprisingly PpRIC-YFP or PpRIC-3xmVenus expression at endogenous levels in protonemal filaments of knockin plants generated on the basis of homologous recombination was below the detection limit of microscopic imaging. To investigate the intracellular distribution of a YFP-PpRIC fusion protein (Figure 3A), estradiol-titratable expression at the lowest detectable level was therefore employed, which was about 10-fold higher than endogenous Pp*RIC* expression (Figures S3A and S3B). In apical initial cells of chloronemal and caulonemal filaments, as well as of rhizoids, YFP-PpRIC accumulated at the plasma membrane specifically within a region that largely overlapped with the apical plasma membrane domain labeled by YFP-PpROP1. However, in contrast to YFP-PpROP1, YFP-PpRIC did not detectably associate with the plasma membrane along cross walls separating apical from subapical cells but strongly accumulated in the nucleus. The latter observation is consistent with nuclear staining in moderately labeled PpRIC-GUS reporter plants (see Figure 2D) as well as with PpRIC containing two predicted NLSs (Figures 1 and 3C). YFP-PpRIC accumulation in the nucleoplasm and the nucleolus was confirmed by co-localization analysis using constitutively expressed chromatin (PpH2B-mCHERRY) and

(F) Different tissues of mature PpRIC-GUS reporter plants (left to right): gametophore (scale bar, 1 mm), antheridium (scale bar, 20 μm), archegonium (scale bar, 100 μm), and sporophyte (scale bar, 1 mm).

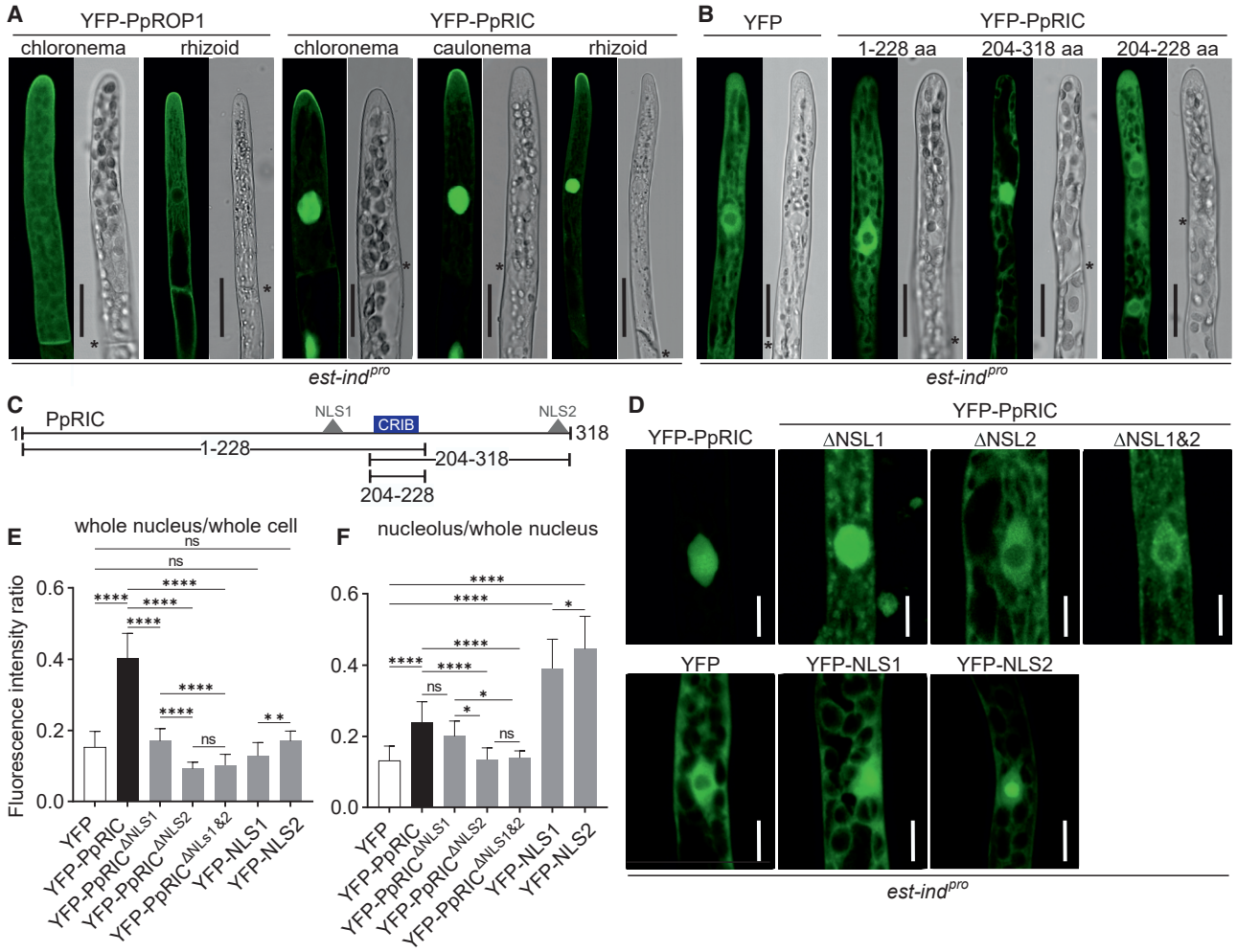

Figure 3. PpRIC co-localizes with PpROP1 and in addition accumulates in the nucleus depending on two predicted NLSs

(A and B) Green: medial confocal optical sections through apical initial cells of protonemal filaments (A and B) or rhizoids (A) displaying estradiol-titratable expression at minimal detectable level of the indicated full-length (A) or truncated (B) YFP fusion proteins, or of free YFP. Distribution patterns were highly reproducible ($n \geq 20$). Grayscale: transmitted light reference images (Nomarski). Scale bars, 25 μm (protonemal cells) and 50 μm (rhizoid cells).

(C) Overlap of the PpRIC fragments analyzed in (B) with the PpRIC CRIB domain and NLSs.

(D) Projections of serial confocal optical sections thorough subapical protonemal cells displaying estradiol-titratable expression at minimal detectable expression levels of free YFP or of YFP fused to WT PpRIC, PpRIC with mutated NLSs, or isolated PpRIC NLSs. Scale bars, 10 μm.

(E and F) Quantitative analysis of the relative integrated fluorescence intensity of the following parts of cells imaged as described in (D): whole cell (including nucleus; entire cell, not just the section shown in D), whole nucleus (including nucleolus), and nucleolus. Plots show fluorescence intensity ratios "whole nucleus/whole cell" (E) and "nucleolus/whole nucleus" (F) computed for cells expressing each of the indicated proteins ($n \geq 20$ cells). Error bars denote SD. Statistical analysis by one-way ANOVA/Tukey's test: ns, $p > 0.05$; *$p \leq 0.05$; **$p \leq 0.01$; ****$p \leq 0.0001$.

nucleolar (mRFP-PpFIB) markers (Figure S4A). Imaging of estradiol-induced YFP-PpRIC expression also established nuclear targeting of this fusion protein in gametophores and reproductive organs (Figure S4B).

To identify PpRIC domains required for intracellular targeting, estradiol-titratable expression at the lowest detectable level (Figure S3B) of YFP fused to truncated PpRIC was analyzed (Figure 3B). YFP fused to the isolated CRIB domain of PpRIC ($PpRIC^{204–228}$) or to this domain attached to the N-terminal ($PpRIC^{1–228}$) or the C-terminal ($PpRIC^{204–318}$) rest of the protein, failed to display plasma membrane association (Figure 3B). Interestingly, only YFP-$PpRIC^{204–318}$, which contains NLS2 near the PpRIC C terminus (Figure 3C), effectively accumulated in the nucleolus like full-length YFP-PpRIC, whereas YFP-$PpRIC^{1–228}$ and YFP-$PpRIC^{204–228}$ displayed an intracellular distribution similar to that of free YFP and could only be detected in the nucleoplasm (Figure 3B). With molecular weights of 27 and 31 kDa, free YFP and YFP-$PpRIC^{204–228}$ are below the 40–60 kDa size limit for free diffusion through nuclear pores, whereas import of larger proteins such as YFP-$PpRIC^{1–228}$ (53 kDa) or YFP-$PpRIC^{204–318}$ (41 kDa) into the nucleoplasm generally requires an NLS.[56,57] Some NLSs, apparently

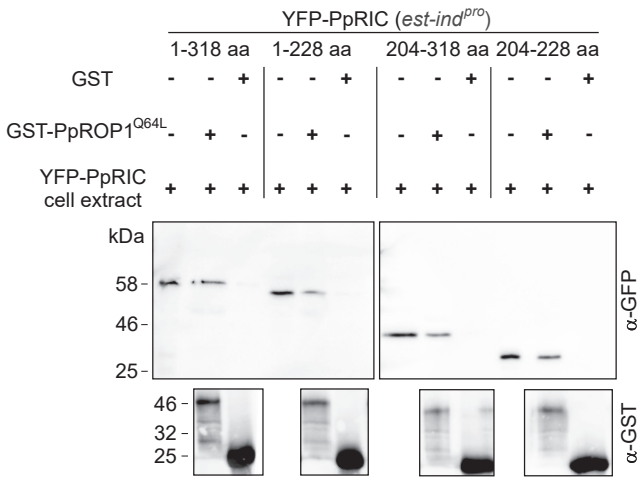

Figure 4. YFP-PpRIC expressed in protonemata physically interacts with recombinant PpROP1^{Q64L}

Pull-down analysis demonstrating co-purification of YFP fused to full-length or truncated PpRIC from extracts of protonemata displaying estradiol-induced expression of these proteins together with GST-tagged GTP-locked PpROP1^{Q64L} purified from *E. coli*. 1–318 amino acids (aa), full-length PpRIC; 1–228 aa, PpRIC N-terminal fragment including CRIB domain; 204–318 aa, PpRIC C-terminal fragment including CRIB domain; 204–228 aa, PpRIC CRIB domain (see Figure 3C). Protonemal extracts and proteins co-purified from these extracts together with GST-PpROP1^{Q64L} or with free GST were analyzed by immunoblotting using α-GFP or α-GST (loading control) antibodies. The experiment was repeated three times with consistent results.

including NLS2 of PpRIC, also mediate targeting to nucleolus which, irrespective of protein size, strictly depends on such signals.[58]

Two predicted NLSs promote PpRIC targeting to the nucleus and the nucleolus

The two predicted NLSs of PpRIC (Figures 1 and 3C) were disrupted by point mutations (ΔNLS1: L181/182A and R183/184A; ΔNLS2: R313A) to unequivocally determine their functions in nuclear and nucleolar targeting. Figure 3D shows maximum projections of serial confocal optical sections through subapical protonemal cells expressing YFP, YFP-PpRIC, YFP-PpRIC$^{\Delta NLS1}$, YFP-PpRIC$^{\Delta NLS2}$, or YFP-PpRIC$^{\Delta NLS1\&2}$ at minimal detectable levels (Figure S3B). Subapical cells divide far less frequently than apical cells,[27,59,60] reducing the possible effects of cell-cycle progression on nuclear or nucleolar targeting. Quantitative analysis of maximum projections generated confirmed active YFP-PpRIC targeting to both the nucleus (Figure 3E) and the nucleolus (Figure 3F). Furthermore, it demonstrated that effective nuclear targeting strongly depends on NLS1 and NLS2, although NLS2 plays a somewhat more prominent role in this process (Figure 3E). By contrast, NLS1 only marginally contributes to nucleolar targeting, which strictly requires NLS2 (Figure 3F). The intracellular distribution of YFP fused to truncated PpRIC shown in Figure 3B is fully consistent with these conclusions. Interestingly, when directly attached to YFP, the isolated NLS1 and NLS2 both failed to substantially enhance import into the nucleus (Figures 3D and 3E) but strongly promoted nucleolar targeting (Figures 3D and 3F). Free YFP and YFP-NLS fusion proteins were expressed at similar levels in the analyzed cells (Figure S3C).

PpRIC physically interacts with PpROP1

Using GTP-locked PpROP1^{Q64L} attached to glutathione S-transferase (GST) and purified from *E. coli*, YFP fused to full-length or truncated PpRIC was pulled down from extracts of protonemata displaying estradiol-induced expression of these proteins (see Figures 3A and 3B). Full-length PpRIC (PpRIC$^{1–318}$), the isolated CRIB domain (PpRIC$^{204–228}$), and the CRIB domain attached to either the N-terminal (PpRIC$^{1–228}$) or C-terminal (PpRIC$^{204–318}$) rest of the protein interacted with PpROP1^{Q64L} essentially equally strongly in these *in vitro* assays (Figure 4). By contrast, full-length PpRIC but none of the truncated forms of this protein co-localized with PpROP1 in apical protonemal cells (Figures 3A and 3B), indicating that specifically *in vivo* PpRIC requires regions flanking the CRIB domain to gain access to PpROP1 effector binding sites within signaling complexes organized by this protein.

PpRIC blocks caulonema differentiation and requires nuclear targeting for this activity

To investigate PpRIC functions in protonemata development, effects on this process of disrupting or overexpressing the Pp*RIC* gene were investigated. Based on homologous recombination, parts of the genomic Pp*RIC* locus were replaced by a marker gene to generate the Pp*ric-1* knockout mutant (Figures S2A and S2B). qRT-PCR analysis confirmed disrupted Pp*RIC* expression in this mutant (Figure 5A). Expression cassettes containing the Pp*RIC* promoter upstream of wild-type (WT) or mutated Pp*RIC* cDNAs were introduced into a neutral region of the Pp*ric-1* genome to obtain complemented lines, which expressed WT PpRIC (Pp*ric-1*$^{comp\text{-}WT}$) or PpRIC$^{\Delta NLS1\&2}$ with mutated NLSs (Pp*ric-1*$^{comp\text{-}\Delta NLS1\&2}$) at essentially endogenous levels (Figure 5A). To generate PpRIC overexpression lines (Pp*RIC*^{OEX}; Figure 5A), an expression cassette containing the Zm*UBQ*^{pro} promoter upstream of the WT Pp*RIC* cDNA was introduced into another neutral region of the WT genome. Furthermore, homologous recombination was employed to reintroduce the genomic Pp*RIC* coding region fused to a YFP cDNA into the disrupted Pp*RIC* locus of the Pp*ric-1* mutant (Figures S2A and S2B). Resulting Pp*ric-1*$^{comp\text{-}YFP\text{-}WT}$ lines contained a Pp*RIC*^{pro}:*YFP*-Pp*RIC*^{gDNA} reporter gene at the Pp*RIC* locus and produced under the control of endogenous expression signals the same YFP-PpRIC fusion protein, which was employed to determine PpRIC intracellular targeting (Figure 3).

Remarkably, completely disrupted or massively enhanced Pp*RIC* expression in 5-day-old chloronemal or caulonemal filaments did not substantially affect the length of subapical cells (Figures 5B and 5C) or overall morphology (Figure 5D), demonstrating that PpRIC does not play a major role in the control of directional cell expansion. Consistent with earlier observations based on RNAi-mediated transient Pp*RIC* knockdown,[61] subapical cells of Pp*ric-1* protonemata displayed a marginal increase in average length, which was statistically significant only in the case of caulonemal filaments (Figures 5B and 5C). Furthermore, PpRIC overexpression appeared to slightly reduce the length of subapical cells specifically in chloronema

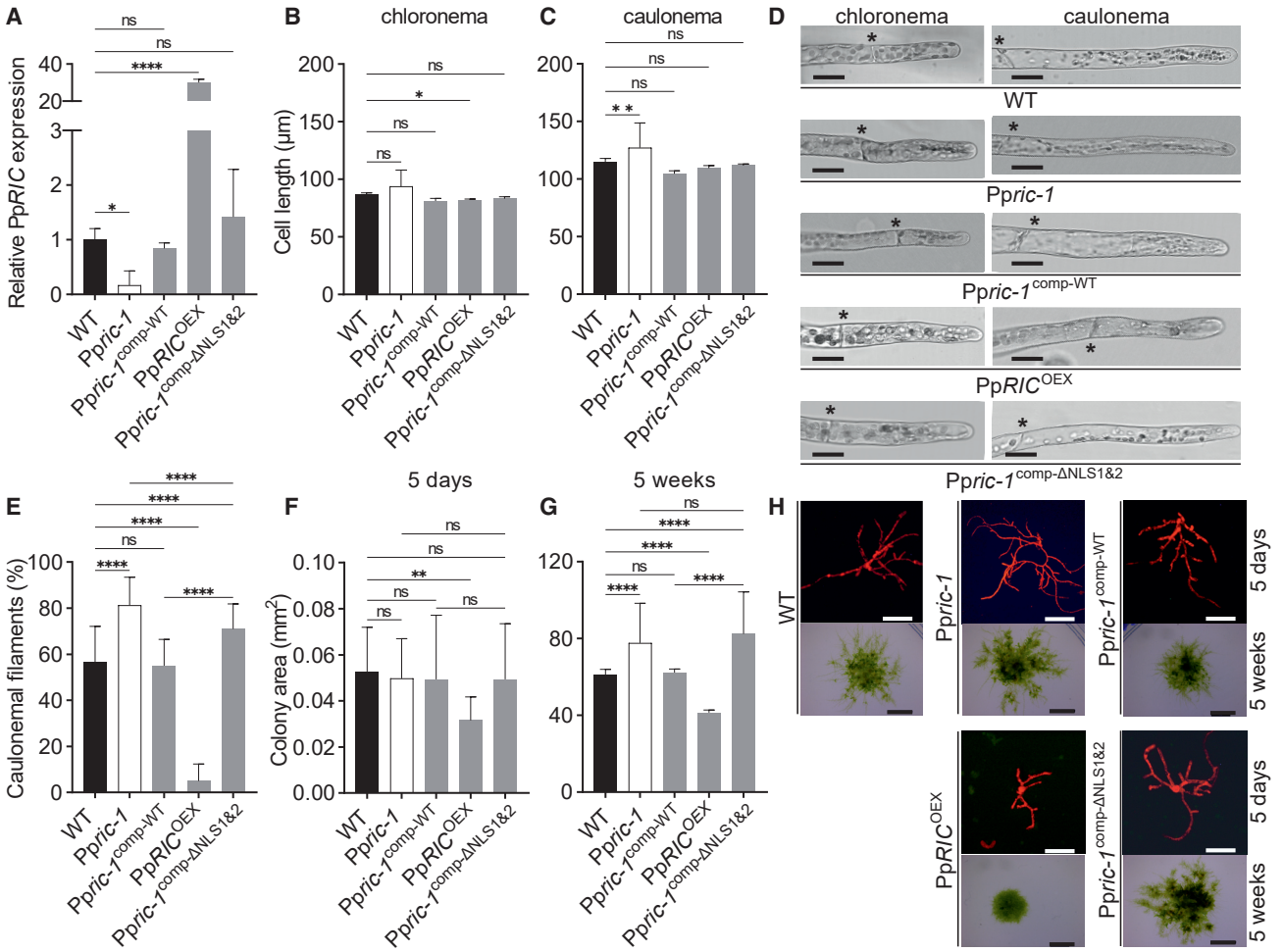

Figure 5. Pp*RIC* disruption or overexpression strongly affects caulonema differentiation, but not directional cell expansion

(A) qRT-PCR analysis of relative Pp*RIC* expression levels in protonemata with the indicated genotypes: WT; Pp*ric-1* knockout mutant; Pp*ric-1*$^{comp\text{-}WT}$ & Pp*ric-1*$^{comp\text{-}\Delta NLS1\&2}$:Pp*ric-1* complemented by PpRIC with intact or mutated NLSs, respectively, expressed at endogenous level (Pp*RIC*^{pro} promoter); and Pp*RIC*^{OEX} transgenic line overexpressing PpRIC in the WT background (Zm*UBQ*^{pro} promoter). Error bars denote SEM. Statistical analysis by one-way ANOVA/Tukey's test: ns, $p > 0.05$; *$p \leq 0.05$; ****$p \leq 0.0001$.

(B and C) Average length of subapical chloronemal (B) or caulonemal (C) cells in 5-day-old protonemata with the indicated genotypes. n = 90 cells/genotype, three independent experiments. Error bars denote SD. Statistical analysis by one-way ANOVA/Tukey's test: ns, $p > 0.05$; *$p \leq 0.05$; **$p \leq 0.01$.

(D) Bright-field micrographs showing tips of 5-day-old protonemal filaments with the indicated genotype. Asterisks indicate cell wall between apical and subapical cell. Scale bars, 25 µm.

(E) Percentage of filaments of 5-day-old protonemata with the indicated genotype, which displayed caulonemal characteristics at the tip (microscopic inspection). n = 90 filaments/genotype, three independent experiments. Error bars denote standard deviation. Statistical analysis by one-way ANOVA/Tukey's test: ns, $p > 0.05$; ****$p \leq 0.0001$.

(F–H) Average size of 5-day-old (F) or 5-week-old (G) colonies with the indicated genotype, as determined by chlorophyll autofluorescence imaging (H, upper panels; 5-day-old colonies) or stereomicroscopic imaging (H, lower panels; 5-week-old colonies). Scale bars, 250 µm (H, upper rows) and 5 mm (H, lower rows). n = 90 colonies/genotype and developmental stage, three independent experiments. Error bars denote SD. Statistical analysis by one-way ANOVA/Tukey's test: ns, $p > 0.05$; **$p \leq 0.01$; ****$p \leq 0.0001$.

(Figure 5B). Altered levels of PpRIC expression had a much more pronounced effect on the development of chloronema to caulonema. Caulonema differentiation was substantially enhanced in the Pp*ric-1* mutant and almost completely blocked in Pp*RIC*^{OEX} plants (Figure 5E), establishing key functions of PpRIC in negatively regulating this process. Consistent with this conclusion, and with caulonema displaying substantially higher growth rates compared with chloronema,[40] the size of 5-day-old and 5-week-old Pp*RIC*^{OEX} colonies was clearly reduced, whereas 5-week-old Pp*ric-1* colonies were significantly enlarged (Figures 5F–5H).

When expressed in Pp*ric-1* at endogenous levels, WT PpRIC (Pp*ric-1*$^{comp\text{-}WT}$) completely complemented the stimulation of caulonema differentiation (Figure 5E) and colony growth (Figure 5G) displayed by this mutant, whereas PpRIC$^{\Delta NLS1\&2}$ (Pp*ric-1*$^{comp\text{-}\Delta NLS1\&2}$) failed to do so (Figures 5E and 5G). Nuclear

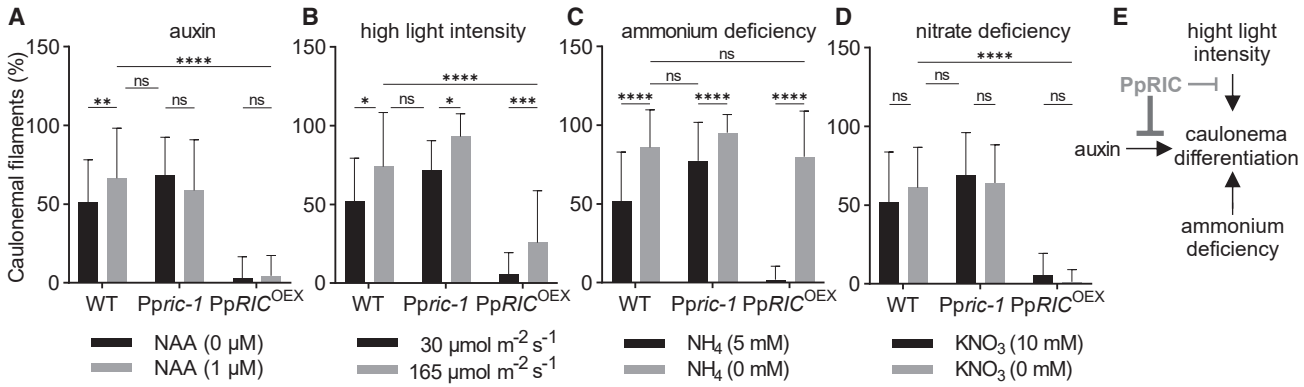

Figure 6. PpRIC differentially interferes with caulonema differentiation induced by auxin, high light intensity, or ammonium deficiency

(A–D) Graphs display the percentage of filaments of 5-day-old protonemata with the indicated genotype, which show caulonemal characteristics at the tip (microscopic inspection). Protonemata were grown under standard conditions (black bars) or under the following non-standard conditions (gray bars): (A) culture medium containing 1 µM NAA (α-naphthalene acetic acid; auxin analog); (B) increased intensity of white light illumination; (C) ammonium-free culture medium; (D) nitrate-free culture medium. n = 90 filaments/genotype and culture condition, three independent experiments. Error bars denote SD. Statistical analysis by two-way ANOVA/Tukey's test: ns, $p > 0.05$; *$p \leq 0.05$; **$p \leq 0.01$; ***$p \leq 0.001$; ****$p \leq 0.0001$.

(E) Model illustrating the induction of caulonema differentiation by auxin, high light intensity, and ammonium deficiency via distinct pathways, which are differentially inhibited by PpRIC.

targeting is therefore clearly required for the ability of PpRIC to block caulonema differentiation. The YFP-PpRIC fusion protein employed to determine PpRIC intracellular localization (Figure 3) also complemented the Pp*ric-1* phenotype (Figure S2C) when generated under the control of endogenous expression signals in Pp*ric-1*$^{comp\text{-}YFP\text{-}WT}$ plants, establishing that N-terminally attached YFP does not disrupt PpRIC function. Enhanced caulonema differentiation as shown by Pp*ric-1* was also exhibited by five additional Pp*ric* knockout mutants generated based on CRISPR-Cas (Pp*ric-2* to Pp*ric-6*), which all contained different frameshift indels within the third Pp*RIC* exon (Figures S2D and S2E).

Estradiol-titratable PpRIC overexpression at maximally induced levels (more than 1,000× endogenous Pp*RIC* expression level; Pp*RIC*$^{OEXest\text{-}ind}$, Figure S5A), which greatly exceeded moderate levels of Zm*UBQ*^{pro}-driven PpRIC overexpression (ca. 40× endogenous Pp*RIC* expression level; Pp*RIC*^{OEX}, Figures 5A and S5A), caused isolated protoplasts to develop into tiny clumps of irregularly shaped cells instead of normal protonemata (Figure S5B). Interestingly, the same phenotype is also caused by total loss of PpROP activity.[25–27] This suggests that massive PpRIC overexpression may prevent access of other effectors to PpROPs, which are required for polarity establishment and for the promotion of directional cell expansion.

PpRIC distinctly inhibits caulonema differentiation induced by auxin, high light intensity, and ammonium deficiency

As previously indicated,[29–31,34,36–38,62] quantitative analysis of caulonema differentiation in WT protonemata under different environmental conditions demonstrated that this process is induced not only by exogenously applied auxins including the synthetic auxin analog α-naphthalene acetic acid (NAA; Figure 6A) but also by environmental factors such as high light intensity (Figure 6B) and ammonium deficiency (Figure 6C). NAA was added to the culture medium at a concentration of 1 µM, as cell growth and morphology were strongly disrupted at higher concentrations. Interestingly, caulonema differentiation was not stimulated when the culture medium was depleted of nitrate instead of ammonium, which serves as an alternative nitrogen source (Figure 6D).

Pp*ric-1* and Pp*RIC*^{OEX} protonemata were also treated with NAA and exposed to high light intensity or ammonium deficiency to investigate whether PpRIC inhibits caulonema differentiation induced by these factors (Figure 6). Remarkably, NAA treatment of WT protonemata induced caulonema differentiation to the same extent as loss of PpRIC expression (Pp*ric-1*), while NAA treatment of Pp*ric-1* protonemata did not further stimulate this process. Moreover, NAA was unable to overcome the nearly complete block of caulonema differentiation resulting from PpRIC overexpression (Pp*RIC*^{OEX}; Figure 6A). Together, these observations strongly suggest that auxin and PpRIC act in a common pathway, which induces caulonema differentiation depending on the balance between auxin stimulation and inhibition by PpRIC. In contrast to auxin, high light intensity and ammonium deficiency further enhanced caulonema differentiation induced by loss of PpRIC expression (Pp*ric-1*; Figures 6B and 6C), and either partially (high light intensity, Figure 6B) or completely (ammonium deficiency, Figure 6C) alleviated the inhibition of this process by PpRIC overexpression (Pp*RIC*^{OEX}). Auxin, high light intensity, and ammonium deficiency therefore appear to induce caulonema differentiation via different pathways, which are distinctly regulated by PpRIC (Figure 6E). Figure S6 shows the morphology of WT, Pp*ric-1*, or Pp*RIC*^{OEX} apical protonemal cells and colonies grown under the different environmental conditions tested.

PpRIC blocks caulonema differentiation downstream of auxin-controlled gene expression

PpRIC could potentially inhibit auxin-induced caulonema differentiation by interfering with any process contributing to the

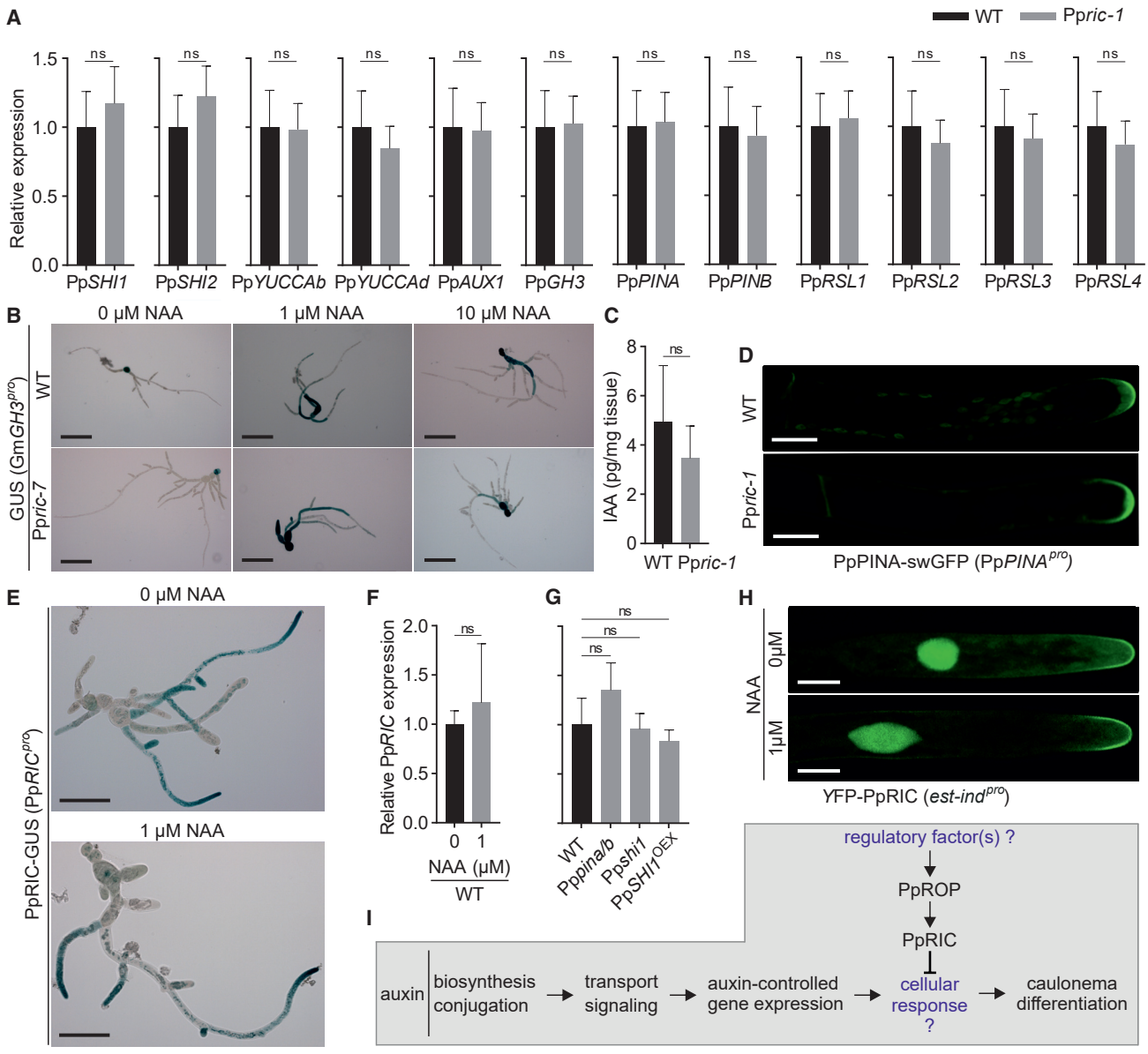

Figure 7. PpRIC blocks caulonema differentiation downstream of auxin-controlled gene expression and appears to display auxin-independent activity

(A–D) PpRIC does not regulate auxin-controlled gene expression, free auxin levels, or auxin transport. (A) qRT-PCR analysis of relative expression levels in 5-day-old WT or Pp*ric-1* protonemata of genes with essential functions in auxin biosynthesis, auxin inactivation by conjugation, auxin transport, auxin signaling, or auxin-induced transcription of genes required for caulonema differentiation. Most of these genes are transcriptionally regulated by auxin. Error bars denote SEM. Statistical analysis by unpaired Student's t test: ns, $p > 0.05$.

(B) Histochemical analysis of GUS activity in 5-day-old protonemata of reporter plants (three independent lines) expressing GUS under the control of the auxin-responsive *Glycine max GH3* promoter (grown in culture medium containing NAA at the indicated concentrations) before (WT, upper row) and after (Pp*ric-7*, lower row) CRISPR-Cas-mediated disruption of the Pp*RIC* gene. Scale bars, 200 µm. (C) Free IAA content of 7-day-old WT and Pp*ric-1* protonemata. Means of three independent measurements. Error bars denote SD. Statistical analysis by unpaired Student's t test: ns, $p > 0.05$. (D) Medial confocal optical sections through apical protonemal cells expressing the auxin transporter PpPINA sandwich-tagged with enhanced GFP[33] under the control of the endogenous Pp*PINA* promoter in the WT or Pp*ric-1* background. Distribution patterns in both backgrounds were indistinguishable and highly reproducible ($n \geq 20$). Scale bars, 10 µm.

(E–H) PpRIC expression and intracellular distribution are auxin independent. (E) Histochemical analysis of GUS activity in 5-day-old protonemata of reporter plants (two independent lines, see Figure 2D) expressing a PpRIC-GUS fusion protein under the control of the PpRIC promoter, which were grown in culture medium containing NAA at the indicated concentrations. Scale bars, 100 µm. (F and G) qRT-PCR analysis of relative Pp*RIC* expression levels (F) in 5-day-old WT protonemata grown in the presence of NAA at the indicated concentrations, or (G) in 7-day-old protonemata containing auxin (IAA) at endogenous (WT), increased (Pp*pina/b*, Pp*SHI1*^{OEX}), or reduced (Pp*shi1*) levels. Error bars denote SEM. Statistical analysis by unpaired Student's t test (F) or one-way ANOVA/Tukey's test

(legend continued on next page)

control of gene expression by this hormone. In fact, the AtROP effectors AtRIC1 and AtRIC4 regulate auxin transport by modulating the plasma membrane distribution of *Arabidopsis* PIN-family auxin efflux carriers.[19–21] However, qRT-PCR analysis (Figure 7A) showed that Pp*ric-1* protonemata display essentially normal expression levels of various genes with key functions in one of the following processes: (1) auxin biosynthesis (Pp*SHI1*, Pp*SHI2*, Pp*YUCCAb*, Pp*YUCCAd*[32]); (2) auxin inactivation by conjugation (Pp*GH3*[63]); (3) auxin transport (Pp*PINA*, Pp*PINB*[33]); (4) auxin signaling (Pp*AUX1*[34]); or (5) auxin-induced transcription of genes required for caulonema differentiation (Pp*RSL1*, Pp*RSL2*, Pp*RSL3*, Pp*RSL4*[64,65]). The analyzed genes not only play important roles in auxin-mediated control of gene expression; with few exceptions (Pp*SHI1*, Pp*SHI2*, Pp*YUCCAb*), they are also transcriptionally regulated by this process.[31,32,34,65]

qRT-PCR data shown in Figure 7A were corroborated by histochemical analysis of GUS activity in 5-day-old transgenic protonemata expressing GUS under the control of the *Glycine max GH3* promoter (Gm*GH3*^{pro}:*GUS*[66]), which reports local stimulation of auxin-controlled gene expression (Figure 7B). CRISPR-Cas-mediated Pp*RIC* disruption (Pp*ric-7*, Figure S2F) had no detectable effects on the level, distribution, or NAA-induced stimulation of GUS activity in these protonemata (Figure 7B). Interestingly, in all analyzed protonemata GUS activity displayed a pronounced base-to-tip gradient, consistent with earlier observations in protonemata containing a similar Gm*GH3*^{pro}:*GFP-GUS* construct or expressing the conceptually different auxin response reporter PpR2D2.[67]

Consistent with the observation that Pp*RIC* disruption does not affect the expression of genes, which are required for auxin biosynthesis or conjugation and/or are transcriptionally controlled by this hormone (Figures 7A and 7B), essentially normal levels of endogenous free auxin (IAA[68]) were measured in 7-day-old Pp*ric-1* protonemata (Figure 7C). Furthermore, Pp*ric-1* protonemal filaments appear to display normal tip-directed auxin transport, as these filaments (1) contain WT levels of transcripts encoding PpPINA and PpPINB (Figure 7A), which are essential for this process,[33] and (2) display no defects in the expression level or intracellular distribution of PpPINA sandwich-tagged with enhanced GFP (Figure 7D), which was expressed under the control of the endogenous Pp*PINA* promoter (Pp*PINA*^{prom}:Pp*PINA-swGFP*[33]).

In summary, encompassing characterization of Pp*ric-1* protonemata neither provided any indications of altered auxin biosynthesis, conjugation, transport, or signaling nor revealed changes in auxin-responsive gene expression (Figure 7). PpRIC therefore appears to block auxin-induced caulonema differentiation by directly interfering with an unknown cellular response required for this process, which is activated downstream of auxin-controlled gene expression.

Auxin does not regulate PpRIC expression or intracellular distribution

Auxin could potentially induce caulonema differentiation by downregulating PpRIC activity, which appears to block this process downstream of auxin-controlled gene expression. In fact, auxin was reported to modulate the activity of different AtROP and AtRIC proteins to regulate polarized cell expansion in *Arabidopsis*.[41,51,69] Moreover, endogenous PpRIC protein levels (reported by Pp*RIC*^{pro}:Pp*RIC*^{gDNA}-*GUS* expression, see Figure 2D) and auxin responsiveness (indicated by Gm*GH3*^{pro}:*GUS* expression, see Figure 7B)[67] display oppositely oriented gradients in protonemal filaments, indicating that auxin may downregulate PpRIC expression. However, no effect of exogenously applied NAA, or of genetic manipulations enhancing or reducing endogenous auxin (IAA) accumulation, on PpRIC expression were detected in 5-day-old protonemata. Levels and distribution of GUS activity in PpRIC-GUS reporter lines (Pp*RIC*^{pro}:Pp*RIC*^{gDNA}-*GUS*, see Figure 2D) were not noticeably altered in the presence of 1 μM NAA (Figure 7E). Furthermore, qRT-PCR analysis (Figures 7F and 7G) established that Pp*RIC* transcript levels were not substantially affected (1) by treatment with 1 μM NAA, (2) in Pp*ina/b* mutants lacking Pp*PINA* and Pp*PINB* expression, which are defective in IAA transport and contain increased levels of this hormone,[33] (3) in a Pp*SHI1*^{OEX} line overexpressing the transcription factor PpSHI1, which also overaccumulates IAA,[32] or (4) in a Pp*shi1* knockout mutant, which displays reduced IAA concentrations.[32] Furthermore, not only PpRIC expression (Figures 7E and 7F) but also the intracellular distribution of YFP-PpRIC in apical protonemal initial cells (see Figure 3A) appeared unaffected in the presence of 1 μM NAA (Figure 7H).

Even though PpRIC expression (Figures 7E–7G) and intracellular distribution (Figure 7H) seem to be auxin independent, this hormone could possibly modulate PpRIC activity by stimulating unidentified post-translational modifications. However, currently available data provide no evidence of such regulatory mechanisms and are consistent with the following hypothesis: auxin-induced caulonema differentiation appears to be attenuated by unknown factors, which target PpROP signaling to stimulate PpRIC-mediated inhibition of an unidentified cellular response that is activated downstream of auxin-controlled gene expression to bring about caulonema differentiation (Figure 7I).

DISCUSSION

PpRIC is functionally distinct from flowering plant RICs and inhibits caulonema differentiation possibly in response to rapid alkalization factor perception

A key function of ROP GTPases in flowering plants[12,13] and *P. patens*[25–27] is the promotion of directional cell expansion. Downstream of ROP activation, different *Arabidopsis* AtRICs regulate

(G): ns, $p > 0.05$. (H) Medial confocal optical sections through apical protonemal cells displaying estradiol-titratable YFP-PpRIC expression at minimal detectable level (see Figure 3A), which were grown in the presence of NAA at the indicated concentrations. Distribution patterns in the presence or absence of NAA were indistinguishable and highly reproducible ($n \geq 20$). Scale bars, 10 μm.

(I) Model suggesting co-regulation of caulonema differentiation by auxin and by unknown regulatory factors, which target PpROP signaling to modulate PpRIC-mediated inhibition of this process.

this process by modulating cytoskeletal organization. Pollen tube tip growth depends on destabilization of apical F-actin by AtRIC1[52] and AtRIC3,[50] which needs to be balanced by AtRIC4-stimulated F-actin assembly.[50] During leaf pavement cell morphogenesis, AtRIC4 promotes cortical F-actin formation required for lobe outgrowth, whereas AtRIC1 stabilizes microtubular structures that limit cell expansion in the indentations between lobes.[51] Additional functions of flowering plant RICs in other ROP-controlled cellular processes have also been identified: AtRIC1 and AtRIC4 modulate membrane traffic to control auxin transport,[19–21] AtRIC7 negatively regulates exocyst activity required for stomatal opening,[17,18] and HvRIC171 promotes pathogen susceptibility based on unknown mechanisms.[22]

As PpRIC shares little sequence or structural similarity with any AtRIC outside of the common CRIB domain (Figures 1 and S1), RIC functions in *P. patens* and *Arabidopsis* are likely to be strikingly different. In fact, knocking out Pp*RIC* expression does not disrupt tip growth of apical protonemal cells (Figures 5A–5D), although this process depends on PpROPs,[25–27] which appear to recruit PpRIC to the apical growth site (Figures 3A and 4). Consistent with this finding, apical cells of short chloronemal filaments undergo tip growth in the absence of detectable PpRIC expression (Figure 2D).

Our data demonstrate that rather than promoting tip growth, PpRIC plays an important role in negatively regulating caulonema differentiation. The recent observation that *P. patens* knockout mutants missing the small secreted signaling proteins PpRALF1 and/or PpRALF2 (rapid alkalization factors) also display enhanced caulonema differentiation[70] further supports an important role of PpROP-dependent PpRIC activation in the negative regulation of this process. AtRALF1, a close homolog of PpRALF1, stimulates ROP signaling in *Arabidopsis* root hairs by activating the receptor-like kinase AtFERONIA,[71,72] which is represented in *P. patens* by three close homologs.[70]

PpRIC contributes to the maintenance of apical initial cell identity

As outlined in the introduction, apical initial cells at the tip of chloronema and caulonema play pivotal roles in protonemal development. The emergence of apical initial cells represents a key invention during the evolution of multicellular land plants from unicellular algae.[62] RHO family small GTPases typically govern cell differentiation or behavior by coordinating different underlying cellular processes via the interaction with multiple effectors.[73,74] It therefore appears conceivable that PpROPs may play central roles in the maintenance of the identity of apical chloronemal initial cells based on their ability to integrate the control of tip growth, caulonema differentiation, and possibly also cell division, another process regulated by RHO family small GTPases in different cell types.[75,76] Apart from PpRIC, the downstream effectors employed by PpROPs for this purpose remain to be identified. ROPs must be expected to activate substantially different downstream signaling in *P. patens* and *Arabidopsis*, not only because RICs appear to have clearly distinct functions in these two organisms but also because homologs of other ROP effectors required for tip growth in flowering plants are missing in *P. patens*.[11]

Caulonema differentiation is subject to complex regulation by different factors

The induction of caulonema differentiation by exogenously applied auxin has been clearly documented in previous studies.[29–31] By contrast, the stimulation of this process by high light and ammonium deficiency has been discussed in the literature[36–38] but was much less thoroughly investigated. Our quantitative analyses establish that both these environmental factors in fact induce caulonema differentiation at least as strongly as auxin treatment (Figures 6A–6C). Furthermore, they demonstrate that, contrary to suggestions in the literature,[36] this process is not affected by nitrate deficiency (Figure 6D). Interestingly, the regulation of caulonema differentiation by light of different spectral composition appears to be complex. Although this process is promoted by high-intensity white light (Figure 6B),[38] it appears to be negatively regulated by activated blue-light receptors.[30]

Remarkably, caulonema differentiation induced by auxin, high light, or ammonium deficiency is differentially negatively regulated by PpRIC (Figures 6A–6C). Although this indicates that each of these factors induces caulonema differentiation via a completely independent pathway (Figure 6E), our data also support a slightly more complex model. High light may induce caulonema differentiation by stimulating an independent pathway that is not regulated by PpRIC together with the auxin pathway, which is effectively blocked by this protein. This scenario is also consistent with our observation that high light further stimulates enhanced caulonema differentiation displayed by Pp*ric-1* mutants and partially alleviates the block of this process resulting from PpRIC overexpression (Figure 6B).

Apical initial cells appear to exhibit predetermined, PpRIC-restricted competence to undergo caulonema differentiation in response to stimulated auxin signaling

Interestingly, auxin responsiveness displays a pronounced base-to-tip gradient in protonemal filaments with lowest levels detected at the tip (Figure 7E).[67] Consequently, caulonema differentiation is not simply triggered specifically in apical initial cells by maximally induced auxin-controlled gene expression but must depend on the predetermined competence of these cells to respond to stimulated auxin signaling. PpROP-dependent PpRIC activity in apical initial cells appears to define the threshold level of auxin stimulation required for caulonema differentiation. Interactions between auxin and ROP signaling are also essential for the control of important developmental processes in flowering plants,[19,41,42] indicating that interplay between these two major signaling pathways plays an evolutionarily conserved central role in plant development.

PpRIC is unlikely to block auxin-induced caulonema differentiation by interfering with F-actin remodeling required for enhanced tip growth

Caulonema differentiation coincides with enhanced tip growth,[40] is abolished in *P. patens* mutants displaying reduced tip growth as a result of defective F-actin regulation,[77,78] and was proposed to generally depend on auxin-induced remodeling of cytoplasmic F-actin structures.[62] Based on these observations, cytoplasmic F-actin remodeling required for enhanced tip growth

could potentially correspond to the unknown cellular response, which PpRIC negatively regulates to block auxin-induced caulonema differentiation (Figure 7I). Although this hypothesis cannot be entirely excluded based on currently available evidence, for the following reasons it appears unlikely: (1) the length of mature subapical chloronemal and caulonemal cells was not substantially affected in Pp*ric* knockout mutants or by Pp*RIC* overexpression (Figures 5A–5D); (2) *Arabidopsis* RICs with demonstrated ability to modulate F-actin organization are structurally clearly distinct from PpRIC (Figure 1) and, as discussed above, promote rather than block tip growth; (3) nuclear targeting is essential for the ability of PpRIC to block caulonema differentiation (Figures 5E and 5G); and (4) PpRIC differentially interferes with caulonema differentiation depending on the inducing factor, rather than generally blocking this process (Figure 6).

The further functional characterization of PpRIC requires the identification of post-translational modifications, interaction partners, and possible target genes

In apical initial cells of protonemal filaments and rhizoids, PpRIC co-localizes with interacting PpROPs at the plasma membrane at the tip and in addition displays nuclear accumulation (Figures 3A and 4), which is required for PpRIC functions in restricting caulonema differentiation (Figures 5E and 5G). We are currently investigating whether GTP-bound PpROPs promote post-translational modifications of PpRIC at the apical plasma membrane, which may activate this protein and stimulate its transfer to the nucleus. Furthermore, to enhance our understanding of molecular and nuclear PpRIC functions, attempts are under way to identify PpRIC interaction partners and to compare transcriptional profiles associated with distinct PpRIC expression levels. Another interesting question to be addressed is the dependence of PpRIC functions on nucleolar targeting, which is mediated primarily by NLS2 (Figures 3D–3F).

The rapid evolution and diversification of the RIC family in flowering plants may be a consequence of the emergence of distinct reproductive structures and functions

Remarkably, the RIC family rapidly structurally evolved, expanded, and diversified with the emergence of flowering plants (Figures 1 and S1). Although the higher rate of evolution displayed by flowering plants as compared with gymnosperms or bryophytes[79] has presumably contributed to this phenomenon, it is unlikely to be solely responsible. The striking structural conservation of the RIC family from mosses to gymnosperms strongly suggests that RICs exert similar essential functions in these land plants. Apparently, these functions and the underlying conserved RIC structure were no longer required in flowering plants, enabling RIC proteins to structurally and functionally diversify.

Although the study presented here focuses on the role of PpRIC in the control of caulonema differentiation, it has also established strong and highly specific expression of this protein in antheridia as well as parts of archegonia (Figure 2F), multicellular organs required for the production of male or female gametes, respectively. These observations strongly suggest additional PpRIC functions in sexual reproduction, which remain to be further characterized. Flowering plants substantially differ from other land plants with respect to reproductive structures and functions.[80–82] Antheridia and archegonia, which were increasingly reduced during land plant evolution, no longer form clearly discernible distinct organs in flowering plants.[83] It therefore appears conceivable that important roles played by RICs in the reproduction of land plants with more ancestral features may have been replaced by other functions in flowering plants.

Conclusions

The ancient CRIB-domain ROP effector PpRIC needs to be targeted to the nucleus to mediate crosstalk between ROP and auxin signaling, which is required for the maintenance of chloronemal apical initial cell identity. These findings represent important insight into not only ROP-dependent downstream signaling and the adaptation of this process during land plant evolution but also the genetic control of *P. patens* development. Supporting data pave the way for highly interesting future research including: (1) the further characterization of molecular mechanisms underlying PpRIC functions based on the identification of post-translational modifications, interaction partners, and possible target genes; (2) the investigation of additional PpRIC functions in caulonema, rhizoids, and reproductive organs; and (3) the identification of novel effectors, which unlike PpRIC are essential for PpROP-controlled directional cell expansion in *P. patens*.

Limitations of this study

As our research focuses on different aspects of *P. patens* protonemal development, the study presented here addresses PpRIC functions during this process, although higher expression levels indicate possible key roles of PpRIC also in gametophore and sporophyte ontogenesis. To initiate PpRIC functional characterization, we thoroughly investigated the phylogenetic context of this protein and its role in the inhibition of apical initial cell differentiation, leaving important aspects of molecular mechanisms underlying this process to be explored by future studies. Without encompassing analysis of possible effects of post-translational modifications on PpRIC activity, regulation of this activity by auxin cannot be entirely excluded. Further investigation of interactions between PpROP and PpRIC based on live-cell imaging could potentially provide important additional information concerning *in vivo* sites of these interactions. The interpretation of data demonstrating a tip-focused PpRIC expression gradient in protonemal filaments, which are based on histochemical analysis of PpRIC-GUS expression driven by the Pp*RIC* promoter, needs to take into account possible differential stabilization of PpRIC by the attached GUS tag in distinct cell types.

STAR★METHODS

Detailed methods are provided in the online version of this paper and include the following:

- KEY RESOURCES TABLE
- RESOURCE AVAILABILITY

SUPPLEMENTAL INFORMATION

Supplemental information can be found online at https://doi.org/10.1016/j.celrep.2023.112130.

ACKNOWLEDGMENTS

We are thankful to Mitsuyasu Hasebe (NIBB, Okazaki, Japan) for the plasmid pPGX8, to Ralf Reski (University of Freiburg, Germany) for a Gm*GH3*^{pro}:*GUS* construct, and to Fabien Nogué (Université Paris-Saclay, Versailles, France) for the plasmids pDONR207 and pAct-CAS9, as well as for providing a CRISPR/Cas mutagenesis protocol. Furthermore, we thank Claudia Erbar (University of Heidelberg, Germany) for providing expertise in land plant evolution, Pierre-François Perroud for the plasmid pTHUBI and for invaluable technical advice, and Mattias Thelander (Swedish University of Agricultural Sciences, Uppsala, Sweden) for the plasmids Pp*PINA*^{prom}:Pp*PINA-swGFP* and pMT123, the Pp*pina/b* and Pp*shi1* knockout mutants, and the transgenic Pp*SHI1*^{OEX} overexpression line as well as for many helpful discussions. Finally, we would like to acknowledge excellent technical support provided by Roger Granbom (Umeå Plant Science Center, Umeå, Sweden), Vanessa Schmidt (University of Erlangen-Nuremberg, Germany), Jennifer Schuster (University of Erlangen-Nuremberg, Germany), and Deborah Baku (University of Erlangen-Nuremberg, Germany). The work was supported by funding from the Swedish Research Council (VR, 2016-05180; D.M.E.), the Knut and Alice Wallenberg Foundation (KAW 2016.0341 and KAW 2016.0352; K.L.), and the Swedish Governmental Agency for Innovation Systems (VINNOVA 2016-00504; K.L.). Confocal microscopy relied on major equipment sponsored by the German Research Foundation (DFG, INST 90/1074-1 FUGG; B.K.).

AUTHOR CONTRIBUTIONS

Conceptualization, M.N., A.L.B., and B.K.; methodology, M.N., A.L.B., and D.M.E.; formal analysis, M.N., A.L.B., D.M.E., and B.K.; investigation, M.N., A.L.B., D.M.E., S.S., F.S., L.B., W.D., C.E., A.B., and K.L; resources, M.N., A.L.B., and B.K.; writing – original draft, M.N., D.M.E., and B.K.; writing – review & editing, M.N., D.M.E., and B.K.; visualization, M.N., D.M.E., and B.K.; supervision, M.N. and B.K.; project administration, B.K.; funding acquisition, D.M.E., K.L., and B.K.

DECLARATION OF INTERESTS

The authors declare no competing interests.

INCLUSION AND DIVERSITY

We support inclusive, diverse, and equitable conduct of research.

Received: June 16, 2022
Revised: December 3, 2022
Accepted: February 1, 2023
Published: February 14, 2023

REFERENCES

1. Etienne-Manneville, S., and Hall, A. (2002). Rho GTPases in cell biology. Nature *420*, 629–635.
2. Kawano, Y., Kaneko-Kawano, T., and Shimamoto, K. (2014). Rho family GTPase-dependent immunity in plants and animals. Front. Plant Sci. *5*, 522.
3. Cherfils, J., and Zeghouf, M. (2013). Regulation of small GTPases by GEFs, GAPs, and GDIs. Physiol. Rev. *93*, 269–309.
4. Hodge, R.G., and Ridley, A.J. (2016). Regulating Rho GTPases and their regulators. Nat. Rev. Mol. Cell Biol. *17*, 496–510.
5. Bishop, A.L., and Hall, A. (2000). Rho GTPases and their effector proteins. Biochem. J. *348*, 241–255.
6. Nielsen, E. (2020). The small GTPase superfamily in plants: a conserved regulatory module with novel functions. Annu. Rev. Plant Biol. *71*, 247–272.
7. Wu, G., Gu, Y., Li, S., and Yang, Z. (2001). A genome-wide analysis of Arabidopsis Rop-linteractive CRIB motif–containing proteins that act as Rop GTPase targets. Plant Cell *13*, 2841–2856.
8. Lavy, M., Bloch, D., Hazak, O., Gutman, I., Poraty, L., Sorek, N., Sternberg, H., and Yalovsky, S. (2007). A novel ROP/RAC effector links cell polarity, root-meristem maintenance, and vesicle trafficking. Curr. Biol. *17*, 947–952.
9. Li, S., Gu, Y., Yan, A., Lord, E., and Yang, Z.-B. (2008). RIP1 (ROP interactive partner 1)/ICR1 marks pollen germination sites and may act in the ROP1 pathway in the control of polarized pollen growth. Mol. Plant *1*, 1021–1035.
10. Stephan, O., Cottier, S., Fahlén, S., Montes-Rodriguez, A., Sun, J., Eklund, D.M., Klahre, U., and Kost, B. (2014). RISAP Is a TGN-associated RAC5 effector regulating membrane traffic during polar cell growth in tobacco. Plant Cell *26*, 4426–4447.
11. Eklund, D.M., Svensson, E.M., and Kost, B. (2010). *Physcomitrella patens*: a model to investigate the role of RAC/ROP GTPase signalling in tip growth. J. Exp. Bot. *61*, 1917–1937.
12. Qin, Y., and Yang, Z. (2011). Rapid tip growth: insights from pollen tubes. Semin. Cell Dev. Biol. *22*, 816–824.
13. Kost, B. (2008). Spatial control of Rho (Rac-Rop) signaling in tip-growing plant cells. Trends Cell Biol. *18*, 119–127.
14. Feiguelman, G., Fu, Y., and Yalovsky, S. (2018). ROP GTPases structure-function and signaling pathways. Plant Physiol. *176*, 57–79.
15. Craddock, C., Lavagi, I., and Yang, Z. (2012). New insights into Rho signaling from plant ROP/Rac GTPases. Trends Cell Biol. *22*, 492–501.
16. Scheible, N., and McCubbin, A. (2019). Signaling in pollen tube growth: beyond the tip of the polarity iceberg. Plants *8*, 156.
17. Jeon, B.W., Hwang, J.-U., Hwang, Y., Song, W.-Y., Fu, Y., Gu, Y., Bao, F., Cho, D., Kwak, J.M., Yang, Z., and Lee, Y. (2008). The Arabidopsis

small G protein ROP2 Is activated by light in guard cells and inhibits light-induced stomatal opening. Plant Cell *20*, 75–87.

18. Hong, D., Jeon, B.W., Kim, S.Y., Hwang, J.U., and Lee, Y. (2016). The ROP2 - RIC7 pathway negatively regulates light-induced stomatal opening by inhibiting exocyst subunit Exo70B1 in Arabidopsis. New Phytol. *209*, 624–635.
19. Chen, X., Naramoto, S., Robert, S., Tejos, R., Löfke, C., Lin, D., Yang, Z., and Friml, J. (2012). ABP1 and ROP6 GTPase signaling regulate clathrin-mediated endocytosis in Arabidopsis roots. Curr. Biol. *22*, 1326–1332.
20. Lin, D., Nagawa, S., Chen, J., Cao, L., Chen, X., Xu, T., Li, H., Dhonukshe, P., Yamamuro, C., Friml, J., et al. (2012). A ROP GTPase-dependent auxin signaling pathway regulates the subcellular distribution of PIN2 in Arabidopsis roots. Curr. Biol. *22*, 1319–1325.
21. Nagawa, S., Xu, T., Lin, D., Dhonukshe, P., Zhang, X., Friml, J., Scheres, B., Fu, Y., and Yang, Z. (2012). ROP GTPase-dependent actin microfilaments promote PIN1 polarization by localized Iinhibition of clathrin-dependent endocytosis. PLoS Biol. *10*, e1001299.
22. Schultheiss, H., Preuss, J., Pircher, T., Eichmann, R., and Hückelhoven, R. (2008). Barley RIC171 interacts with RACB in planta and supports entry of the powdery mildew fungus. Cell Microbiol. *10*, 1815–1826.
23. Rensing, S.A., Lang, D., Zimmer, A.D., Terry, A., Salamov, A., Shapiro, H., Nishiyama, T., Perroud, P.F., Lindquist, E.A., Kamisugi, Y., et al. (2008). The Physcomitrella genome reveals evolutionary insights into the conquest of land by plants. Science *319*, 64–69.
24. Rensing, S.A., Goffinet, B., Meyberg, R., Wu, S.-Z., and Bezanilla, M. (2020). The moss *Physcomitrium* (*Physcomitrella*) *patens*: a model organism for non-seed plants. Plant Cell *32*, 1361–1376.
25. Burkart, G.M., Baskin, T.I., and Bezanilla, M. (2015). A family of ROP proteins that suppresses actin dynamics, and is essential for polarized growth and cell adhesion. J. Cell Sci. *128*, 2553–2564.
26. Cheng, X., Mwaura, B.W., Chang Stauffer, S.R., and Bezanilla, M. (2020). A fully functional ROP fluorescent fusion protein reveals roles for this GTPase in subcellular and tissue-level patterning. Plant Cell *32*, 3436–3451.
27. Yi, P., and Goshima, G. (2020). Rho of plants GTPases and cytoskeletal elements control nuclear positioning and asymmetric cell division during *Physcomitrella patens* branching. Curr. Biol. *30*, 2860–2868.e3.
28. Le Bail, A., Schulmeister, S., Perroud, P.F., Ntefidou, M., Rensing, S.A., and Kost, B. (2019). Analysis of the localization of fluorescent PpROP1 and PpROP-GEF4 fusion proteins in moss protonemata based on genomic "knock-in" and estradiol-titratable expression. Front. Plant Sci. *10*, 456.
29. Ashton, N.W., Grimsley, N.H., and Cove, D.J. (1979). Analysis of gametophytic development in the moss, *Physcomitrella patens*, using auxin and cytokinin resistant mutants. Planta *144*, 427–435.
30. Imaizumi, T., Kadota, A., Hasebe, M., and Wada, M. (2002). Cryptochrome light signals control development to suppress auxin sensitivity in the moss *Physcomitrella patens*. Plant Cell *14*, 373–386.
31. Jang, G., and Dolan, L. (2011). Auxin promotes the transition from chloronema to caulonema in moss protonema by positively regulating PpRSL1and PpRSL2 in *Physcomitrella patens*. New Phytol. *192*, 319–327.
32. Eklund, D.M., Thelander, M., Landberg, K., Ståldal, V., Nilsson, A., Johansson, M., Valsecchi, I., Pederson, E.R.A., Kowalczyk, M., Ljung, K., et al. (2010). Homologues of the *Arabidopsis thaliana* SHI/STY/LRP1 genes control auxin biosynthesis and affect growth and development in the moss *Physcomitrella patens*. Development *137*, 1275–1284.
33. Viaene, T., Landberg, K., Thelander, M., Medvecka, E., Pederson, E., Feraru, E., Cooper, E.D., Karimi, M., Delwiche, C.F., Ljung, K., et al. (2014). Directional auxin transport mechanisms in early diverging land plants. Curr. Biol. *24*, 2786–2791.
34. Lavy, M., Prigge, M.J., Tao, S., Shain, S., Kuo, A., Kirchsteiger, K., and Estelle, M. (2016). Constitutive auxin response in Physcomitrella reveals complex interactions between Aux/IAA and ARF proteins. Elife *5*, e13325.
35. Wang, R., and Estelle, M. (2014). Diversity and specificity: auxin perception and signaling through the TIR1/AFB pathway. Curr. Opin. Plant Biol. *21*, 51–58.
36. Reski, R. (1998). Development, genetics and molecular biology of mosses. Bot. Acta *111*, 1–15.
37. Schween, G., Gorr, G., Hohe, A., and Reski, R. (2003). Unique tissue-specific cell cycle in Physcomitrella. Plant Biol. (Stuttg). *5*, 50–58.
38. Thelander, M., Olsson, T., and Ronne, H. (2005). Effect of the energy supply on filamentous growth and development in *Physcomitrella patens*. J. Exp. Bot. *56*, 653–662.
39. Menand, B., Yi, K., Jouannic, S., Hoffmann, L., Ryan, E., Linstead, P., Schaefer, D.G., and Dolan, L. (2007). An ancient mechanism controls the development of cells with a rooting function in land plants. Science *316*, 1477–1480.
40. Menand, B., Calder, G., and Dolan, L. (2007). Both chloronemal and caulonemal cells expand by tip growth in the moss Physcomitrella patens. J. Exp. Bot. *58*, 1843–1849.
41. Xu, T., Wen, M., Nagawa, S., Fu, Y., Chen, J.-G., Wu, M.-J., Perrot-Rechenmann, C., Friml, J., Jones, A.M., and Yang, Z. (2010). Cell surface- and Rho GTPase-based auxin signaling controls cellular interdigitation in Arabidopsis. Cell *143*, 99–110.
42. Nakamura, M., and Grebe, M. (2018). Outer, inner and planar polarity in the Arabidopsis root. Curr. Opin. Plant Biol. *41*, 46–53.
43. Cheng, S., Xian, W., Fu, Y., Marin, B., Keller, J., Wu, T., Sun, W., Li, X., Xu, Y., Zhang, Y., et al. (2019). Genomes of subaerial Zygnematophyceae provide insights into land plant evolution. Cell *179*, 1057–1067.e14.
44. Harholt, J., Moestrup, Ø., and Ulvskov, P. (2016). Why plants were terrestrial from the beginning. Trends Plant Sci. *21*, 96–101.
45. Puttick, M.N., Morris, J.L., Williams, T.A., Cox, C.J., Edwards, D., Kenrick, P., Pressel, S., Wellman, C.H., Schneider, H., Pisani, D., and Donoghue, P.C.J. (2018). The interrelationships of land plants and the nature of the ancestral embryophyte. Curr. Biol. *28*, 733–745.e2.
46. Rensing, S.A. (2018). Plant evolution: phylogenetic relationships between the earliest land plants. Curr. Biol. *28*, R210–R213.
47. Harris, B.J., Harrison, C.J., Hetherington, A.M., and Williams, T.A. (2020). Phylogenomic evidence for the monophyly of bryophytes and the reductive evolution of stomata. Curr. Biol. *30*, 2001–2012.e2.
48. Su, D., Yang, L., Shi, X., Ma, X., Zhou, X., Hedges, S.B., and Zhong, B. (2021). Large-Scale phylogenomic analyses reveal the monophyly of bryophytes and neoproterozoic origin of land plants. Mol. Biol. Evol. *38*, 3332–3344.
49. Moore, M.J., Bell, C.D., Soltis, P.S., and Soltis, D.E. (2007). Using plastid genome-scale data to resolve enigmatic relationships among basal angiosperms. Proc. Natl. Acad. Sci. USA *104*, 19363–19368.
50. Gu, Y., Fu, Y., Dowd, P., Li, S., Vernoud, V., Gilroy, S., and Yang, Z. (2005). A Rho family GTPase controls actin dynamics and tip growth via two counteracting downstream pathways in pollen tubes. J. Cell Biol. *169*, 127–138.
51. Fu, Y., Gu, Y., Zheng, Z., Wasteneys, G., and Yang, Z. (2005). Arabidopsis interdigitating cell growth requires two antagonistic pathways with opposing action on cell morphogenesis. Cell *120*, 687–700.
52. Zhou, Z., Shi, H., Chen, B., Zhang, R., Huang, S., and Fu, Y. (2015). Arabidopsis RIC1 severs actin filaments at the apex to regulate pollen tube growth. Plant Cell *27*, 1140–1161.
53. Ortiz-Ramírez, C., Hernandez-Coronado, M., Thamm, A., Catarino, B., Wang, M., Dolan, L., Feijó, J.A., and Becker, J.D. (2016). A transcriptome atlas of *Physcomitrella patens* provides insights into the evolution and development of land plants. Mol. Plant *9*, 205–220.
54. Perroud, P.F., Haas, F.B., Hiss, M., Ullrich, K.K., Alboresi, A., Amirebrahimi, M., Barry, K., Bassi, R., Bonhomme, S., Chen, H., et al. (2018). The

Physcomitrella patens gene atlas project: large-scale RNA-seq based expression data. Plant J. *95*, 168–182.

55. Fernandez-Pozo, N., Haas, F.B., Meyberg, R., Ullrich, K.K., Hiss, M., Perroud, P.-F., Hanke, S., Kratz, V., Powell, A.F., Vesty, E.F., et al. (2020). PEATmoss (Physcomitrella Expression Atlas Tool): a unified gene expression atlas for the model plant *Physcomitrella patens*. Plant J. *102*, 165–177.
56. Wang, R., and Brattain, M.G. (2007). The maximal size of protein to diffuse through the nuclear pore is larger than 60 kDa. FEBS Lett. *581*, 3164–3170.
57. Weis, K. (2003). Regulating access to the genome: nucleocytoplasmic transport throughout the cell cycle. Cell *112*, 441–451.
58. Martin, R.M., Ter-Avetisyan, G., Herce, H.D., Ludwig, A.K., Lättig-Tünnemann, G., and Cardoso, M.C. (2015). Principles of protein targeting to the nucleolus. Nucleus *6*, 314–325.
59. Cove, D.J., and Knight, C.D. (1993). The moss *Physcomitrella patens*, a model system with potential for the study of plant reproduction. Plant Cell *5*, 1483–1488.
60. Uenaka, H., Wada, M., and Kadota, A. (2005). Four distinct photoreceptors contribute to light-induced side branch formation in the moss *Physcomitrella patens*. Planta *222*, 623–631.
61. Bascom, C., Jr., Burkart, G.M., Mallett, D.R., O'Sullivan, J.E., Tomaszewski, A.J., Walsh, K., and Bezanilla, M. (2019). Systematic survey of the function of ROP regulators and effectors during tip growth in the moss *Physcomitrella patens*. J. Exp. Bot. *70*, 447–457.
62. Jaeger, R., and Moody, L.A. (2021). A fundamental developmental transition in *Physcomitrium patens* is regulated by evolutionarily conserved mechanisms. Evol. Dev. *23*, 123–136.
63. Ludwig-Müller, J., Jülke, S., Bierfreund, N.M., Decker, E.L., and Reski, R. (2009). Moss (*Physcomitrella patens*) GH3 proteins act in auxin homeostasis. New Phytol. *181*, 323–338.
64. Jang, G., Yi, K., Pires, N.D., Menand, B., and Dolan, L. (2011). RSL genes are sufficient for rhizoid system development in early diverging land plants. Development *138*, 2273–2281.
65. Pires, N.D., Yi, K., Breuninger, H., Catarino, B., Menand, B., and Dolan, L. (2013). Recruitment and remodeling of an ancient gene regulatory network during land plant evolution. Proc. Natl. Acad. Sci. USA *110*, 9571–9576.
66. Bierfreund, N.M., Reski, R., and Decker, E.L. (2003). Use of an inducible reporter gene system for the analysis of auxin distribution in the moss *Physcomitrella patens*. Plant Cell Rep. *21*, 1143–1152.
67. Thelander, M., Landberg, K., and Sundberg, E. (2019). Minimal auxin sensing levels in vegetative moss stem cells revealed by a ratiometric reporter. New Phytol. *224*, 775–788.
68. Ashton, N.W., Schulze, A., Hall, P., and Bandurski, R.S. (1985). Estimation of indole-3-acetic acid in gametophytes of the moss, *Physcomitrella patens*. Planta *164*, 142–144.
69. Pan, X., Fang, L., Liu, J., Senay-Aras, B., Lin, W., Zheng, S., Zhang, T., Guo, J., Manor, U., Van Norman, J., et al. (2020). Auxin-induced signaling protein nanoclustering contributes to cell polarity formation. Nat. Commun. *11*, 3914.
70. Ginanjar, E.F., Teh, O.K., and Fujita, T. (2022). Characterisation of rapid alkalinisation factors in *Physcomitrium patens* reveals functional conservation in tip growth. New Phytol. *233*, 2442–2457.
71. Duan, Q., Kita, D., Li, C., Cheung, A.Y., and Wu, H.-M. (2010). FERONIA receptor-like kinase regulates RHO GTPase signaling of root hair development. Proc. Natl. Acad. Sci. USA *107*, 17821–17826.
72. Zhu, S., Estévez, J.M., Liao, H., Zhu, Y., Yang, T., Li, C., Wang, Y., Li, L., Liu, X., Pacheco, J.M., et al. (2020). The RALF1–FERONIA complex phosphorylates eIF4E1 to promote protein synthesis and polar root hair growth. Mol. Plant *13*, 698–716.
73. Kang, I.S., Jang, J.S., and Kim, C. (2020). Opposing roles of hematopoietic-specific small GTPase Rac2 and the guanine nucleotide exchange factor Vav1 in osteoclast differentiation. Sci. Rep. *10*, 7024.
74. Sugiyama, Y., Nagashima, Y., Wakazaki, M., Sato, M., Toyooka, K., Fukuda, H., and Oda, Y. (2019). A Rho-actin signaling pathway shapes cell wall boundaries in Arabidopsis xylem vessels. Nat. Commun. *10*, 468.
75. Stöckle, D., Herrmann, A., Lipka, E., Lauster, T., Gavidia, R., Zimmermann, S., and Müller, S. (2016). Putative RopGAPs impact division plane selection and interact with kinesin-12 POK1. Nat. Plants *2*, 16120.
76. Clark, S.E., Williams, R.W., and Meyerowitz, E.M. (1997). The CLAVATA1 gene encodes a putative receptor kinase that controls shoot and floral meristem size in Arabidopsis. Cell *89*, 575–585.
77. Finka, A., Saidi, Y., Goloubinoff, P., Neuhaus, J.-M., Zrÿd, J.P., and Schaefer, D.G. (2008). The knock-out of ARP3a gene affects F-actin cytoskeleton organization altering cellular tip growth, morphology and development in the moss *Physcomitrella patens*. Cell Motil. Cytoskelet. *65*, 769–784.
78. Perroud, P.-F., and Quatrano, R.S. (2006). The role of ARPC4 in tip growth and alignment of the polar axis in filaments of *Physcomitrella patens*. Cell Motil. Cytoskelet. *63*, 162–171.
79. Linde, A.-M., Eklund, D.M., Cronberg, N., Bowman, J.L., and Lagercrantz, U. (2021). Rates and patterns of molecular evolution in bryophyte genomes, with focus on complex thalloid liverworts. Mol. Phylogenet. Evol. *165*, 107295.
80. Mathews, S., and Kramer, E.M. (2012). The evolution of reproductive structures in seed plants: a re-examination based on insights from developmental genetics. New Phytol. *194*, 910–923.
81. Leslie, A.B., Simpson, C., and Mander, L. (2021). Reproductive innovations and pulsed rise in plant complexity. Science *373*, 1368–1372.
82. Friedman, W.E., and Floyd, S.K. (2001). Perspective: the origin of flowering plants and their reproductive biology? A tale of two phylogenies. Evolution *55*, 217–231.
83. Yuan, L., Liu, Z., Song, X., Jernstedt, J., and Sundaresan, V. (2018). The gymnosperm ortholog of the angiosperm central cell-specification gene CKI1 provides an essential clue to endosperm origin. New Phytol. *218*, 1685–1696.
84. Collonnier, C., Epert, A., Mara, K., Maclot, F., Guyon-Debast, A., Charlot, F., White, C., Schaefer, D.G., and Nogué, F. (2017). CRISPR-Cas9-mediated efficient directed mutagenesis and RAD51-dependent and RAD51-independent gene targeting in the moss *Physcomitrella patens*. Plant Biotechnol. J. *15*, 122–131.
85. Perroud, P.-F., Cove, D.J., Quatrano, R.S., and McDaniel, S.F. (2011). An experimental method to facilitate the identification of hybrid sporophytes in the moss *Physcomitrella patens* using fluorescent tagged lines. New Phytol. *191*, 301–306.
86. Hiwatashi, Y., Obara, M., Sato, Y., Fujita, T., Murata, T., and Hasebe, M. (2008). Kinesins are indispensable for interdigitation of phragmoplast microtubules in the moss *Physcomitrella patens*. Plant Cell *20*, 3094–3106.
87. Kubo, M., Imai, A., Nishiyama, T., Ishikawa, M., Sato, Y., Kurata, T., Hiwatashi, Y., Reski, R., and Hasebe, M. (2013). System for stable β-estradiol-inducible gene expression in the moss physcomitrella patens. PLoS One *8*, e77356.
88. Lavy, M., Prigge, M.J., Tigyi, K., and Estelle, M. (2012). The cyclophilin DIAGEOTROPICA has a conserved role in auxin signaling. Development *139*, 1115–1124.
89. Thelander, M., Olsson, T., and Ronne, H. (2004). Snf1-related protein kinase 1 is needed for growth in a normal day–night light cycle. EMBO J. *23*, 1900–1910.
90. Thelander, M., Nilsson, A., Olsson, T., Johansson, M., Girod, P.-A., Schaefer, D.G., Zrÿd, J.P., and Ronne, H. (2007). The moss genes PpSKI1 and PpSKI2 encode nuclear SnRK1 interacting proteins with homologues in vascular plants. Plant Mol. Biol. *64*, 559–573.

91. Dalal, J., Yalamanchili, R., La Hovary, C., Ji, M., Rodriguez-Welsh, M., Aslett, D., Ganapathy, S., Grunden, A., Sederoff, H., and Qu, R. (2015). A novel gateway-compatible binary vector series (PC-GW) for flexible cloning of multiple genes for genetic transformation of plants. Plasmid *81*, 55–62.

92. Campbell, R.E., Tour, O., Palmer, A.E., Steinbach, P.A., Baird, G.S., Zacharias, D.A., and Tsien, R.Y. (2002). A monomeric red fluorescent protein. Proc. Natl. Acad. Sci. USA *99*, 7877–7882.

93. Grebnev, G., Cvitkovic, M., Fritz, C., Cai, G., Smith, A.-S., and Kost, B. (2020). Quantitative structural organization of bulk apical membrane traffic in pollen tubes. Plant Physiol. *183*, 1559–1585.

94. Schindelin, J., Arganda-Carreras, I., Frise, E., Kaynig, V., Longair, M., Pietzsch, T., Preibisch, S., Rueden, C., Saalfeld, S., Schmid, B., et al. (2012). Fiji: an open-source platform for biological-image analysis. Nat. Methods *9*, 676–682.

95. Bailey, T.L., Boden, M., Buske, F.A., Frith, M., Grant, C.E., Clementi, L., Ren, J., Li, W.W., and Noble, W.S. (2009). MEME Suite: tools for motif discovery and searching. Nucleic Acids Res. *37*, W202–W208.

96. Altschul, S.F., Gish, W., Miller, W., Myers, E.W., and Lipman, D.J. (1990). Basic local alignment search tool. J. Mol. Biol. *215*, 403–410.

97. One Thousand Plant Transcriptomes Initiative; Barker, M.S., Carpenter, E.J., and Deyholos, M.K. (2019). One thousand plant transcriptomes and the phylogenomics of green plants. Nature *574*, 679–685.

98. Berardini, T.Z., Reiser, L., Li, D., Mezheritsky, Y., Muller, R., Strait, E., and Huala, E. (2015). The Arabidopsis Information Resource: Making and mining the "gold standard" annotated reference plant genome. Genesis *53*, 474–485.

99. Concordet, J.-P., and Haeussler, M. (2018). CRISPOR: intuitive guide selection for CRISPR/Cas9 genome editing experiments and screens. Nucleic Acids Res. *46*, W242–W245.

100. Proost, S., Van Bel, M., Vaneechoutte, D., Van de Peer, Y., Inzé, D., Mueller-Roeber, B., and Vandepoele, K. (2015). Plaza 3.0: an access point for plant comparative genomics. Nucleic Acids Res. *43*, D974–D981.

101. Goodstein, D.M., Shu, S., Howson, R., Neupane, R., Hayes, R.D., Fazo, J., Mitros, T., Dirks, W., Hellsten, U., Putnam, N., and Rokhsar, D.S. (2012). Phytozome: a comparative platform for green plant genomics. Nucleic Acids Res. *40*, D1178–D1186.

102. Grigoriev, I.V., Nordberg, H., Shabalov, I., Aerts, A., Cantor, M., Goodstein, D., Kuo, A., Minovitsky, S., Nikitin, R., Ohm, R.A., et al. (2012). The genome portal of the department of energy joint genome institute. Nucleic Acids Res. *40*, D26–D32.

103. Nguyen Ba, A.N., Pogoutse, A., Provart, N., and Moses, A.M. (2009). NLStradamus: a simple hidden markov model for nuclear localization signal prediction. BMC Bioinf. *10*, 202.

104. Gouy, M., Guindon, S., and Gascuel, O. (2010). SeaView version 4: a multiplatform graphical user interface for sequence alignment and phylogenetic tree building. Mol. Biol. Evol. *27*, 221–224.

105. Sievers, F., Wilm, A., Dineen, D., Gibson, T.J., Karplus, K., Li, W., Lopez, R., McWilliam, H., Remmert, M., Söding, J., et al. (2011). Fast, scalable generation of high-quality protein multiple sequence alignments using Clustal Omega. Mol. Syst. Biol. *7*, 539.

106. Guindon, S., Dufayard, J.-F., Lefort, V., Anisimova, M., Hordijk, W., and Gascuel, O. (2010). New algorithms and methods to estimate maximum-likelihood phylogenies: assessing the performance of PhyML 3.0. Syst. Biol. *59*, 307–321.

107. Ashton, N.W., and Cove, D.J. (1977). The isolation and preliminary characterisation of auxotrophic and analogue resistant mutants of the moss, *Physcomitrella patens*. Mol. Gen. Genet. *154*, 87–95.

108. Grimsley, N.H., Ashton, N.W., and Cove, D.J. (1977). The production of somatic hybrids by protoplast fusion in the moss, *Physcomitrella patens*. Mol. Gen. Genet. *154*, 97–100.

109. Cove, D.J., Perroud, P.-F., Charron, A.J., McDaniel, S.F., Khandelwal, A., and Quatrano, R.S. (2009). The moss *Physcomitrella patens*: a novel model system for plant development and genomic studies. Cold Spring Harb. Protoc. *2009*, pdb.emo115.

110. Sayers, E.W., Bolton, E.E., Brister, J.R., Canese, K., Chan, J., Comeau, D.C., Connor, R., Funk, K., Kelly, C., Kim, S., et al. (2022). Database resources of the national center for biotechnology information. Nucleic Acids Res. *50*, D20–D26.

111. Lefort, V., Longueville, J.-E., and Gascuel, O. (2017). SMS: Smart model selection in PhyML. Mol. Biol. Evol. *34*, 2422–2424.

112. Snapp, E. (2005). Design and use of fluorescent fusion proteins in cell biology. Curr. Protoc. Cell Biol. *27*, 21.4.1–21.4.13.

113. Green, M.R., and Sambrook, J. (2012). Molecular Cloning: A Laboratory Manual, 4th Edition (Cold Spring Harbor Laboratory Press).

114. Schaefer, D.G., and Zrÿd, J.P. (1997). Efficient gene targeting in the moss *Physcomitrella patens*. Plant J. *11*, 1195–1206.

115. Okano, Y., Aono, N., Hiwatashi, Y., Murata, T., Nishiyama, T., Ishikawa, T., Kubo, M., and Hasebe, M. (2009). A polycomb repressive complex 2 gene regulates apogamy and gives evolutionary insights into early land plant evolution. Proc. Natl. Acad. Sci. USA *106*, 16321–16326.

116. Schaefer, D., Zryd, J.-P., Knight, C.D., and Cove, D.J. (1991). Stable transformation of the moss *Physcomitrella patens*. Mol. Gen. Genet. *226*, 418–424.

117. Katzen, F. (2007). Gateway® recombinational cloning: a biological operating system. Expert Opin. Drug Discov. *2*, 571–589.

118. Ormö, M., Cubitt, A.B., Kallio, K., Gross, L.A., Tsien, R.Y., and Remington, S.J. (1996). Crystal structure of the *Aequorea victoria* green fluorescent protein. Science *273*, 1392–1395.

119. Shaner, N.C., Campbell, R.E., Steinbach, P.A., Giepmans, B.N.G., Palmer, A.E., and Tsien, R.Y. (2004). Improved monomeric red, orange and yellow fluorescent proteins derived from Discosoma sp. red fluorescent protein. Nat. Biotechnol. *22*, 1567–1572.

120. Cormack, B.P., Valdivia, R.H., and Falkow, S. (1996). FACS-optimized mutants of the green fluorescent protein (GFP). Gene *173*, 33–38.

121. Le Bail, A., Scholz, S., and Kost, B. (2013). Evaluation of reference genes for RT qPCR analyses of structure-specific and hormone regulated gene expression in *Physcomitrella patens* gametophytes. PLoS One *8*, e70998.

122. Vidali, L., Augustine, R.C., Kleinman, K.P., and Bezanilla, M. (2007). Profilin is essential for tip growth in the moss *Physcomitrella patens*. Plant Cell *19*, 3705–3722.

123. Andersen, S.U., Buechel, S., Zhao, Z., Ljung, K., Novák, O., Busch, W., Schuster, C., and Lohmann, J.U. (2008). Requirement of B2-type cyclin-dependent kinases for meristem integrity in *Arabidopsis thaliana*. Plant Cell *20*, 88–100.

STAR★METHODS

KEY RESOURCES TABLE

REAGENT or RESOURCE	SOURCE	IDENTIFIER
Antibodies		
anti-GST	Merck	Cat# G1160; RRID: AB_259845
anti-GFP	Merck	Cat# G1544; RRID: AB_439690
IgG HRP (anti-mouse)	Promega	Cat# W402B; RRID: W4021
IgG HRP (anti-rabbit)	Promega	Cat# W401B; RRID: W4011
Bacterial and virus strains		
E. coli BL21 (DE3)	Widely distributed	N/A
E. coli DH5α	Widely distributed	N/A
E. coli BL21 (DE3): tac^{pro}:*GST*-Pp*ROP1*^{Q64L}	This paper	BL21-pFAU312
E. coli BL21 (DE3): tac^{pro}:*GST*	This paper/VWR	BL21-pGEX4T2
Chemicals, peptides, and recombinant proteins		
Ammonium tartrate	Merck	Cat# P5655
Magnesium sulfate	Roth	Cat# P027.1
Potassium Phosphate	Roth	Cat# P5655
Potassium nitrate	Roth	Cat# P021.1
Calcium chloride	Roth	Cat# HN04.3
Potassium chloride	Roth	Cat# 6781.3
Potassium bromide	Roth	Cat# A137.1
Potassium iodine	Roth	Cat# 0323.1
Lithium chloride	Roth	Cat# 3739.1
Tin(II) chloride	AppliChem	Cat# A5181
Zinc sulfate	Merck	Cat# 108883
Agar-agar	Roth	Cat# 4807.3
Agar high-strength	Merck	Cat# A9799
Cellophane discs	AA Packaging	Cat# 325P
Vancomycin	Duchefa	Cat# V0155.0025
Driselase	Merck	Cat# D9515
Polyethylene glycol Mw6000	Roth	Cat# 0158.2
D-Mannitol	AppliChem	Cat# 142067.0914
Hygromycin B	Roth	Cat# CP13.4
G418	Merck	Cat# A1720
Zeocin	Thermo Fisher	Cat# R25001
Dimethyl sulfoxide	Roth	Cat# 4720.3
β-estradiol	Merck	Cat# E8875
^{13}C6-IAA	Cambridge Isotope Laboratories	Cat# CLM-1896-PK
Naphthalene acetic acid	Merck	Cat# N0640
Sodium hydroxide	Roth	Cat# 6771.1
Disodium hydrogen phosphate	Roth	Cat# T883.1
Potassium hexacyanoferrate(III)	Merck	Cat# 244023
Potassium hexacyanoferrate(II)	Merck	Cat# P3289
Triton X-100	Merck	Cat# 108603
5-Bromo-4-chloro-3-indolyl-β-D-glucuronide cyclohexylammonium salt	Goldbio	Cat# G1281C1

(*Continued on next page*)

Continued

REAGENT or RESOURCE	SOURCE	IDENTIFIER
Isopropyl-β-D-thiogalactopyranoside	Roth	Cat# 2316.4
Tris ultrapure	AppliChem	Cat# A1086,5000
Hydrochloric acid	vWR	Cat# 20252.420
Sodium chloride	Roth	Cat# 3957.2
Ethylenediaminetetraacetic acid	Merck	Cat# 108418
Lysozyme	Roth	Cat# 8259.1
Sodium deoxycholate	Merck	Cat# D6750
Nonidet P-40 substitute	G-Biosciences	Cat# 786-511
Rothipherese Gel 30	Roth	Cat# 3029.1
AscI	Nippon Genetics	Cat# FG-AscI
BamHI	Nippon Genetics	Cat# FG-BamHI
DpnI	Nippon Genetics	Cat# FG-DpnI
EcoRI	Nippon Genetics	Cat# FG-EcoRI
HindIII	Nippon Genetics	Cat# FG-HindIII
HpaI	New England Biolabs	Cat# R0105
NgomIV	Nippon Genetics	Cat# FG-NgoMIV
NotI	New England Biolabs	Cat# R3189
PacI	New England Biolabs	Cat# R0547
SalI	New England Biolabs	Cat# R3138
XbaI	New England Biolabs	Cat# R0145
XhoI	New England Biolabs	Cat# R0146
XmaI	New England Biolabs	Cat# FG-XmaI
Critical commercial assays		
PCRBio HS VeriFi Polymerase	Nippon Genetics	Cat# PB10.47–01
Phusion Polymerase	New England Biolabs	Cat# M0530S
FastGene Optima HotStart ReadyMix	Nippon Genetics	Cat# LS29
Gateway LR clonase II	Life Technologies	Cat# 11791020
Gateway BP clonase II	Life Technologies	Cat# 11789020
In-Fusion HD Cloning Plus	Takara	Cat# 638909
Nucleospin RNA Plus	Macherey-Nagel	Cat# 740984.250
iScript cDNA Synthesis kit	Bio-Rad	Cat# 1708891
SsoAdvanced Universal SYBR Green Supermix	Bio-Rad	Cat# 1725275
Nucleon PhytoPure	Merck	Cat# GERPN8511
Complete protease inhibitor mix	Merck	Cat# 11697498001
Bradford assay	Merck	Cat# B-6916
MagneGST Glutathione Particles	Promega	Cat# V8611
Experimental models: Organisms/strains		
Physcomitrium patens, Gransden	Ashton and Cove, 1977	N/A
P. patens: Ppric-1 (Pp*RIC* knock-out mutant, homologous recombination)	This paper	Pp-pSLU74
P. patens: Ppric-2; Ppric-3; Ppric-4; Ppric-5; Ppric-6 (Pp*RIC* knock-out mutants, CRISPR/Cas)	This paper	Pp-pFAU709/ pAct-CAS9
P. patens: Ppric-1$^{comp-WT}$ (complemented Ppric-1, Pp*RIC*^{pro}:Pp*RIC* in neutral region)	This paper	Pp-pSLU74/ pFAU342
P. patens: Ppric-1$^{comp-\Delta NLS1\&2}$ (complemented Ppric-1, Pp*RIC*^{pro}:Pp*RIC*$^{\Delta NLS1\&2}$ in neutral region)	This paper	Pp-pSLU74/ pFAU550

(*Continued on next page*)

Continued

REAGENT or RESOURCE	SOURCE	IDENTIFIER
P. patens: Ppric-1$^{comp-YFP-WT}$ (complemented Ppric-1, Pp*RIC*^{pro}:*YFP*-Pp*RIC*^{gDNA} in Pp*RIC* locus, homologous recombination)	This paper	Pp-pSLU74/ pFAU1211
P. patens: PpRIC-GUS reporter lines (Pp*RIC*^{pro}:Pp*RIC*^{gDNA}-*GUS* in Pp*RIC* locus, homologous recombination)	This paper	Pp-pSLU62
P. patens: Pp*RIC*^{OEX} (Zm*UBQ*^{pro}:Pp*RIC*)	This paper	Pp-pFAU168
P. patens: Pp*RIC*$^{OEXest-ind}$ (*est-ind*^{pro}: Pp*RIC*) [β-estradiol: 1 μM (OEX effects)]	This paper	Pp-pFAU820
P. patens: Zm*UBQ*^{pro}:*GUS*	This paper	Pp-pFAU183
P. patens: *est-ind*^{pro}:*YFP*-Pp*RIC* [β-estradiol: 10^{-2} μM (imaging) or 1 μM (pull down)]	This paper	Pp-pFAU374
P. patens: *est-ind*^{pro}:*YFP*-Pp*RIC*$^{1-228}$ [β-estradiol: 10^{-2} μM (imaging) or 1 μM (pull down)]	This paper	Pp-pFAU375
P. patens: *est-ind*^{pro}:*YFP*-Pp*RIC*$^{204-318}$ [β-estradiol: 10^{-4} μM (imaging) or 1 μM (pull down)]	This paper	Pp-pFAU376
P. patens: *est-ind*^{pro}:*YFP*-Pp*RIC*$^{204-228}$ [β-estradiol: 10^{-4} μM (imaging) or 1 μM (pull down)]	This paper	Pp-pFAU377
P. patens: *est-ind*^{pro}:*YFP*-Pp*RIC*^{ΔNLS1} [β-estradiol: 10^{-5} μM (imaging)]	This paper	Pp-pFAU420
P. patens: *est-ind*^{pro}:*YFP*-Pp*RIC*^{ΔNLS2} [β-estradiol: 10^{-2} μM (imaging)]	This paper	Pp-pFAU500
P. patens: *est-ind*^{pro}:*YFP*-Pp*RIC*$^{ΔNLS1&2}$ [β-estradiol: 10^{-4} μM (imaging)]	This paper	Pp-pFAU505
P. patens: *est-ind*^{pro}:*YFP-NLS1* [β-estradiol: 10^{-2} μM (imaging)]	This paper	Pp-pFAU747
P. patens: *est-ind*^{pro}:*YFP-NLS2* [β-estradiol: 10^{-2} μM (imaging)]	This paper	Pp-pFAU493
P. patens: *est-ind*^{pro}:*YFP* [β-estradiol: 10^{-2} μM (imaging)]	This paper	Pp-pFAU702
P. patens: *est-ind*^{pro}:*YFP*-Pp*RIC*/ *35S*^{pro}:*mRFP*-Pp*FIB* [β-estradiol: 10^{-2} μM (imaging)]	This paper	Pp-pFAU374/ pFAU740
P. patens: *est-ind*^{pro}:*YFP*-PpRIC/ Zm*UBQ10*^{pro}:Pp*H2B-mCHERRY* [β-estradiol: 10^{-2} μM (imaging)	This paper	Pp-pFAU374/pFAU733
P. patens: Gm*GH3*^{pro}:*GUS*	This paper	Pp-pRTGH3::GUS
P. patens: Ppric-7 in Gm*GH3*^{pro}:*GUS* (Pp*RIC* knock-out mutant, CRISPR/Cas, generated in Gm*GH3*^{pro}:*GUS* background)	This paper	Pp-pRTGH3::GUS/pFAU849/ pAct-CAS9
P. patens: Pp*PINA*^{pro}:Pp*PINA-swGFP*	This paper	Pp- p*PINA*^{pro}:Pp*PINA-swGF*
P. patens: Pp*PINA*^{pro}:Pp*PINA-swGFP* in Ppric-1 (Ppric-1 transformed with p*PINA*^{pro}:Pp*PINA-swGF*)	This paper	Pp-pSLU74/p*PINA*^{pro}:Pp*PINA-swGF*
P. patens: Pp*ina/b*	Viaene et al., 2014[33]	N/A
P. patens: Pp*shi1*	Eklund et al., 2010b[32]	N/A
P. patens: Pp*SHI1*^{OEX}	Eklund et al., 2010b[32]	N/A
Oligonucleotides		
Primers for plasmid construction, genotyping or qPCR	This paper	Table S4

(*Continued on next page*)

Continued

REAGENT or RESOURCE	SOURCE	IDENTIFIER
Recombinant DNA		
bacterial and, if applicable, plant resistance expression cassette indicated in brackets: [bacterial; plant]; Amp: Ampicillin, Hyg: Hygromycin; Zeo: Zeocin, G418: Geneticin, Kan: Kanamycin, Chl: Chloramphenicol, Gen: Gentamycin, Spec: Spectinomycin		
plasmid used to generate Pp*ric-1* mutant (homologous recombination: knock-out)	This paper, Figure S2	pSLU74 [Amp^{res}; Hyg^{res}]
plasmid used to generate Pp*RIC*^{pro}:Pp*RIC*^{gDNA}-*GUS* line (homologous recombination: knock-in)	This paper, Figure S2	pSLU62, [Kan^{res}, Zeo^{res}; G418^{res}]
intermediate plasmid 1 to construct pSLU62	This paper	pSLU60 [Kan^{res}; -]
intermediate plasmid 2 to construct pSLU62	This paper	pSLU61 [Kan^{res}; -]
plasmid used to generate Pp*ric-1*$^{comp-YFP-WT}$ line (homologous recombination: knock-in)	This paper, Figure S2	pFAU1211 [Amp^{res}; G418^{res}]
plasmid used to generate Pp*ric-1*$^{comp-WT}$ line (Pp*RIC*^{pro}:Pp*RIC* insertion into Pp*ric-1* neutral region)	This paper	pFAU342 [Kan^{res}; G418^{res}]
plasmid used to generate PpRIC$^{comp-\Delta NLS1\&2}$ line (Pp*RIC*^{pro}:Pp*RIC*$^{\Delta NLS1\&2}$ insertion into Pp*ric-1* neutral region)	This paper	pFAU550 [Kan^{res}; G418^{res}]
pENTR/D vector containing *GUS*(*uidA*) *cDNA*	This paper	pFAU182 [Kan^{res}; -]
plasmid containing Zm*UBQ*^{pro}:*GUS*	This paper	pFAU183 [Amp^{res}; Hyg^{res}]
pENTR/D vector containing Pp*RIC cDNA*	This paper	pFAU166 [Kan^{res}; -]
plasmid containing Zm*Ubq*^{pro}: Pp*RIC* (PpRIC^{OEX})	This paper	pFAU168 [Amp^{res}; Hyg^{res}]
plasmid containing *est-ind*^{pro}: Pp*RIC* (Pp*RIC*$^{OEXest-ind}$)	This paper	pFAU820 [Amp^{res}; Hyg^{res}]
pENTR/D vector containing*YFP-PpRIC* cDNA	This paper	pFAU370 [Kan^{res}; -]
plasmid containing *YFP*-Pp*RIC* cDNA	This paper	pFAU366 [Amp^{res}; -]
plasmid containing *est-ind*^{pro}:*YFP*-Pp*RIC*	This paper	pFAU374 [Amp^{res}; Hyg^{res}]
plasmid containing *est-ind*^{pro}:*YFP*-Pp*RIC*$^{1-228}$	This paper	pFAU375 [Amp^{res}; Hyg^{res}]
plasmid containing *est-ind*^{pro}: *YFP*-Pp*RIC*$^{204-318}$	This paper	pFAU376 [Amp^{res}; Hyg^{res}]
plasmid containing *est-ind*^{pro}: *YFP*-Pp*RIC*$^{204-228}$	This paper	pFAU377 [Amp^{res}; Hyg^{res}]
plasmid containing *est-ind*^{pro}:*YFP*-Pp*RIC*$^{\Delta NLS1}$	This paper	pFAU420 [Amp^{res}; Hyg^{res}]
plasmid containing *est-ind*^{pro}:*YFP*-Pp*RIC*$^{\Delta NLS2}$	This paper	pFAU500 [Amp^{res}; Hyg^{res}]
plasmid containing *est-ind*^{pro}: *YFP*-Pp*RIC*$^{\Delta NLS1\&2}$	This paper	pFAU505 [Amp^{res}; Hyg^{res}]
plasmid containing *est-ind*^{pro}:*YFP-NLS1*	This paper	pFAU747 [Amp^{res}; Hyg^{res}]
plasmid containing *est-ind*^{pro}:*YFP-NLS2*	This paper	pFAU493 [Amp^{res}; Hyg^{res}]
plasmid containing *est-ind*^{pro}:*YFP*	This paper	pFAU702 [Amp^{res}; Hyg^{res}]

(*Continued on next page*)

Continued

REAGENT or RESOURCE	SOURCE	IDENTIFIER
plasmid containing *35S^{pro}:mRFP*-Pp*FIB*	This paper	pFAU740 [Amp^{res}, Kan^{res}; Zeo^{res}]
plasmid containing *ZmUBQ^{pro}*: Pp*H2B-mCHERRY*	This paper	pFAU733 [Kan^{res}; G418^{res}]
E. coli expression vector: *tac^{pro}:GST*	VWR	pGEX4T2 [Amp^{res}; -]
E. coli expression vector: *tac^{pro}:GST*-Pp*ROP1*	This paper	pFAU311 [Amp^{res}; -]
E. coli expression vector: *tac^{pro}*: *GST*-Pp*ROP1^{Q64L}*	This paper	pFAU312 [Amp^{res}; -]
plasmid containing Os*ACT^{pro}*:Sp*Cas9*	Collonnier et al., 2017[84]	pAct-CAS9 [Amp^{res}; -]
vector for sgRNA construction (G418^{res} cassette)	Collonnier et al., 2017[84]	pDONR207-KanR [Gen^{res}; G418^{res}]
Pp*RIC* CRISPR/Cas knock-out sgRNA in pDONR207-KanR	This paper	pFAU709 [Gen^{res}; G418^{res}]
vector for sgRNA construction (G418^{res} cassette of pDONR207-KanR replaced by Hyg^{res} cassette)	This paper	pFAU832 [Gen^{res}; Hyg^{res}]
Pp*RIC* CRISPR/Cas knock-out sgRNA in pFAU832	This paper	pFAU849 [Gen^{res}; Hyg^{res}]
plasmid containing Pp*PINA^{pro}*: Pp*PINA-swGFP*	Viaene et al., 2014[33]	p*PINA^{pro}*:Pp*PINA-swGF* [Amp^{res}; G418^{res}]
plasmid containing Gm*GH3^{pro}:GUS*	Bierfreund et al., 2003[66]	pRTGH3::GUS [Spec^{res}; G418^{res}]
plasmid containing *est^{pro}:YFP*-Pp*ROP1*	Le Bail et al., 2019[28]	pFAU260 [Amp^{res}; Hyg^{res}]
Zm*UBQ^{pro}* expression vector (homologous recombination: insertion into neutral region)	Perroud et al., 2011[85]	pTHUBI [Amp^{res}, Chl^{res}; Hyg^{res}]
35S expression vector (homologous recombination: insertion into neutral region)	Hiwatashi et al., 2008[86]	pCMAK1 [Amp^{res}, Kan^{res}; Zeo^{res}]
est-ind^{pro} expression vector (homologous recombination: insertion into neutral region)	Kubo et al., 2013[87]	pGX8 [Amp^{res}; Hyg^{res}]
cloning vector (homologous recombination: insertion into neutral region)	Lavy et al., 2012[88]	pMP1180 [Kan^{res}; G418^{res}]
P. patens knock-out/knock-in vector (Hyg^{res} cassette)	Thelander et al., 2004[89]	pMT123 [Amp^{res}; Hyg^{res}]
P. patens knock-out/knock-in vector (G418^{res} cassette)	Thelander et al., 2007[90]	pMT164 [Amp^{res}; G418^{res}]
TOPO cloning vector	Thermo Fisher Scientific	pENTR/D-Topo [Kan^{res}; -]
plasmid containing *mCHERRY* cDNA	Dalal et al.2015[91]	pCAMBIA [Kan^{res}; -]
plasmid containing *mRFP* cDNA	Campbell et al. 2002[92]	pNCS-mRFP [Amp^{res}; -]
plasmid containing *GUS*(*uidA*) cDNA	Eklund et al., 2010b[32]	pPpGUS [Kan^{res}, Zeo^{res}; G418^{res}]
plasmid containing *YFP* cDNA	Grebnev et al., 2020[93]	pWEN240 [Amp^{res}; -]
Software and algorithms		
GraphPad Prism 9.4.1	GraphPad	RRID:SCR_000306; https://www.graphpad.com/
Leica Application Suite X v3.5.2 (Leica TCS SP8 DIVE-FALCON confocal microscope)	Leica	RRID:SCR_013673; https://www.leica-microsystems.com/products/microscope-software/p/leica-las-x-ls/
Leica Application Suite Advanced Fluorescence v3.2.09652 (Leica DMI4000B wide-field epifluorescence microscope)	Leica	RRID:SCR_013673; https://www.leica-microsystems.com/products/microscope-software/p/leica-las-x-ls/
Leica Application Suite v4.12.0 (Leica M205FA epifluorescence stereo microscope)	Leica	RRID:SCR_016555; https://www.leica-microsystems.com/products/microscope-software/details/product/leica-application-suite/

(*Continued on next page*)

Continued

REAGENT or RESOURCE	SOURCE	IDENTIFIER
Fiji-ImageJ	Schindelin et al., 2012[94]	RRID:SCR_002285; https://imagej.net/software/fiji/
MEME	Bailey et al., 200[95]	RRID:SCR_001783; https://meme-suite.org/meme/tools/meme
NCBI, BLAST	Altschul et al., 1990[96]	RRID:SCR_008419; https://www.ncbi.nlm.nih.gov/
NCBI, GenBank	Leebens-Mack et al., 2019[97]	RRID:SCR_013288; https://www.ncbi.nlm.nih.gov/genbank/
TAIR	Berardini et al., 2015[98]	RRID:SCR_008419; https://www.arabidopsis.org/
ONEKP	Leebens-Mack et al., 2019[97]	https://db.cngb.org/onekp/
CRISPOR	Concordet and Haeussler, 2018[99]	RRID:SCR_015935; http://crispor.tefor.net/
Gymno PLAZA 1.0	Proost et al., 2014[100]	https://bioinformatics.psb.ugent.be/plaza/versions/gymno-plaza/
Phytozome	Goodstein et al., 2012[101]	RRID:SCR_006507 https://phytozome-next.jgi.doe.gov/
PhycoCosm	Grigoriev et al., 2012[102]	https://phycocosm.jgi.doe.gov/phycocosm/home
NLStradamus	Nguyen Ba et al., 2009[103]	http://www.moseslab.csb.utoronto.ca/NLStradamus/
SeaView v4.7	Gouy et al., 2010[104]	RRID:SCR_015059 http://doua.prabi.fr/software/seaview
Clustal Omega	Sievers et al., 2011[105]	RRID:SCR_001591; https://www.ebi.ac.uk/Tools/msa/clustalo/
PhyML 3.0	Guindon et al., 2010[106]	RRID:SCR_014629; http://www.atgc-monteller.fr/phyml/

Other		
Pp*AUX1*	Phytozome	Phytozome: Pp3c16_22730V3.1
Pp*FIB*	Phytozome	Phytozome: Pp3c5_11200V3.1
Pp*H2B*	Phytozome	Phytozome: Pp3c12_7610V3.1
Pp*PINA*	Phytozome	Phytozome: Pp3c23_10200V3.1
Pp*PINB*	Phytozome	Phytozome: Pp3c24_2970V3.1
Pp*RIC*	Phytozome	Phytozome: Pp3c12_19130V1.1
Pp*ROP1*	Phytozome	Phytozome: Pp3c14_4310V3.1
Pp*ROP2*	Phytozome	Phytozome: Pp3c2_20700V3.1
Pp*ROP3*	Phytozome	Phytozome: Pp3c1_21550V3.1
Pp*ROP4*	Phytozome	Phytozome: Pp3c10_4950V3.1
Pp*RSL1*	Phytozome	Phytozome: Pp3c1_38880V3.1
Pp*RSL2*	Phytozome	Phytozome: Pp3c2_8880V3.1
Pp*RSL3*	Phytozome	Phytozome: Pp3c4_24380V3.1
Pp*RSL4*	Phytozome	Phytozome: Pp3c26_10830V1.1
Pp*SHI1*	Phytozome	Phytozome: Pp3c21_16440
Pp*SHI2*	Phytozome	Phytozome: Pp3c18_8920V3.1
Pp*UBIQUITIN-E2*	Phytozome	Phytozome: Pp3c14_21480V1.1
Pp*YUCCAb*	Phytozome	Phytozome: Pp3c11_11790V1.1
Pp*YUCCAd*	Phytozome	Phytozome: Pp3c2_27740V3.1
Pp*U6* (confers non-coding RNA expression)	Phytozome	Phytozome: Chr01:5,050,307..5050621
Zm*UBQ*	GenBank	GenBank: S94464.1
Gm*GH3*	GenBank	GenBank: X60,033.1
CaMV*35S*^{pro}	GenBank	GenBank: V00141.1

(*Continued on next page*)

Continued

REAGENT or RESOURCE	SOURCE	IDENTIFIER
AtRIC1	This paper	Table S1
AtRIC2	This paper	Table S1
AtRIC3	This paper	Table S1
AtRIC4	This paper	Table S1
AtRIC5	This paper	Table S1
AtRIC6	This paper	Table S1
AtRIC7	This paper	Table S1
AtRIC8	This paper	Table S1
AtRIC9	This paper	Table S1
AtRIC10	This paper	Table S1
AtRIC11	This paper	Table S1
OsRIC1	This paper	Table S1
OsRIC2	This paper	Table S1
OsRIC3	This paper	Table S1
OsRIC4	This paper	Table S1
OsRIC5	This paper	Table S1
OsRIC6	This paper	Table S1
AtrRIC4	This paper	Table S1
AtrRIC10	This paper	Table S1
TbRIC	This paper	Table S1
ArRIC	This paper	Table S1
PsyRIC	This paper	Table S1
PtRIC1	This paper	Table S1
PtRIC2	This paper	Table S1
PsiRIC	This paper	Table S1
PaRIC1	This paper	Table S1
PaRIC2	This paper	Table S1
PmRIC	This paper	Table S1
CmRIC	This paper	Table S1
PvRIC1	This paper	Table S1
PvRIC2	This paper	Table S1
CmRIC1	This paper	Table S1
CmRIC2	This paper	Table S1
CspRIC	This paper	Table S1
partial RIC sequence	This paper	Table S1
DcRIC	This paper	Table S1
OspRIC	This paper	Table S1
OjRIC	This paper	Table S1
partial RIC sequence	This paper	Table S1
ApRIC	This paper	Table S1
partial RIC sequence	This paper	Table S1
AfRIC1	This paper	Table S1
AfRIC2	This paper	Table S1
DlRIC	This paper	Table S1
DwRIC	This paper	Table S1
BsRIC1	This paper	Table S1
BsRIC2	This paper	Table S1
BsRIC3	This paper	Table S1
CfRIC1	This paper	Table S1
CfRIC2	This paper	Table S1

(*Continued on next page*)

Continued

REAGENT or RESOURCE	SOURCE	IDENTIFIER
CfRIC3	This paper	Table S1
DfeRIC	This paper	Table S1
DspRIC	This paper	Table S1
HpRIC	This paper	Table S1
PacRIC	This paper	Table S1
DtRIC	This paper	Table S1
LiRIC1	This paper	Table S1
LiRIC2	This paper	Table S1
partial RIC sequence	This paper	Table S1
LlRIC	This paper	Table S1
NeRIC	This paper	Table S1
partial RIC sequence	This paper	Table S1
partial RIC sequence	This paper	Table S1
PamRIC	This paper	Table S1
PglRIC	This paper	Table S1
PplRIC	This paper	Table S1
PheRIC1	This paper	Table S1
PheRIC2	This paper	Table S1
AteRIC1	This paper	Table S1
AteRIC2	This paper	Table S1
AteRIC3	This paper	Table S1
AalRIC	This paper	Table S1
AniRIC1	This paper	Table S1
AniRIC2	This paper	Table S1
CacRIC1	This paper	Table S1
CacRIC2	This paper	Table S1
MeRIC	This paper	Table S1
NmRIC	This paper	Table S1
PtrRIC1	This paper	Table S1
PtrRIC2	This paper	Table S1
PeRIC1	This paper	Table S1
PeRIC2	This paper	Table S1
VliRIC1	This paper	Table S1
VliRIC2	This paper	Table S1
VapRIC	This paper	Table S1
TacRIC	This paper	Table S1
WsRIC	This paper	Table S1
PgloRIC	This paper	Table S1
AcaRIC	This paper	Table S1
AtoRIC	This paper	Table S1
LjaRIC	This paper	Table S1
PdRIC	This paper	Table S1
SmRIC	This paper	Table S1
SaRIC	This paper	Table S1
SwRIC	This paper	Table S1
SkRIC	This paper	Table S1
SlRIC	This paper	Table S1
SsRIC	This paper	Table S1
SapRIC	This paper	Table S1
SwiRIC	This paper	Table S1

(*Continued on next page*)

Continued

REAGENT or RESOURCE	SOURCE	IDENTIFIER
HsRIC	This paper	Table S1
HseRIC	This paper	Table S1
HlRIC	This paper	Table S1
DoRIC	This paper	Table S1
DdRIC	This paper	Table S1
PcRIC	This paper	Table S1
LaRIC	This paper	Table S1
LdRIC	This paper	Table S1
LanRIC	This paper	Table S1
PpRIC	This paper	Table S1
PcRIC	This paper	Table S1
DfRIC	This paper	Table S1
TlRIC	This paper	Table S1
SfRIC1	This paper	Table S1
SfRIC2	This paper	Table S1
SleRIC	This paper	Table S1
SpaRIC1	This paper	Table S1
SpaRIC2	This paper	Table S1
AruRIC	This paper	Table S1
AroRIC	This paper	Table S1
AaRIC	This paper	Table S1
AhRIC	This paper	Table S1
BaRIC	This paper	Table S1
CcRIC1	This paper	Table S1
CcRIC2	This paper	Table S1
CpRIC	This paper	Table S1
DsRIC	This paper	Table S1
DfoRIC	This paper	Table S1
EsRIC	This paper	Table S1
FaRIC1	This paper	Table S1
FaRIC2	This paper	Table S1
HcRIC	This paper	Table S1
LalRIC1	This paper	Table S1
LalRIC2	This paper	Table S1
LgRIC	This paper	Table S1
LsRIC	This paper	Table S1
NdRIC	This paper	Table S1
OlRIC	This paper	Table S1
PfRIC	This paper	Table S1
PiRIC	This paper	Table S1
PelRIC	This paper	Table S1
RvRIC1	This paper	Table S1
RvRIC2	This paper	Table S1
RsRIC	This paper	Table S1
RcfcRIC	This paper	Table S1
SaqRIC	This paper	Table S1
SprRIC	This paper	Table S1
TpRIC	This paper	Table S1
TdRIC	This paper	Table S1
TaRIC	This paper	Table S1

(*Continued on next page*)

Continued

REAGENT or RESOURCE	SOURCE	IDENTIFIER
SmuRIC	This paper	Table S1
CsRIC	This paper	Table S1
EfRIC	This paper	Table S1
KnRIC	This paper	Table S1
SpRIC	This paper	Table S1

RESOURCE AVAILABILITY

Lead contact

Further information and requests for resources and reagents should be directed to and will be fulfilled by the lead contact, Benedikt Kost (benedikt.kost@fau.de).

Materials availability

Plasmids and *P. patens* lines generated in this study are listed in the key resources table and are available from the lead contact upon request. The key resources table also indicates the chromosome position of the Pp*U6* promoter used to the drive sgRNA expression and lists the accession numbers of all other *P. patens* (Phytozome), *Arabidopsis thaliana* (TAIR), *Zea mays* (GenBank), or *Glycine max* (GenBank) genes investigated or used in the experimental part of this study. The accession numbers of all Pp*RIC* homologs identified by BLAST searches in different genome or transcriptome databases are indicated in Table S1.

Data and code availability

- This paper analyzes existing, publicly available datasets. The websites through which these dataset can be accessed, and if available their PRIDs, are listed in the key resources table.
- This paper does not report original code.
- Any additional information required to reanalyze the data reported in this paper is available from the lead contact upon request.

EXPERIMENTAL MODEL AND SUBJECT DETAILS

Physcomitrium patens

Wild type, transgenic and mutated *Physcomitrium patens* ecotype Gransden (2012)[107] cultures were maintained axenically in 9 cm Petri dishes on solid culture medium at 25°C under continuous white light illumination with an intensity of 30 μmol m^{-2} s^{-1} (standard conditions) or 165 μmol m^{-2} s^{-1} (high light conditions) (TrueDaylight LEDs, Poly Klima). If not indicated otherwise, the culture medium was solidified with 0.7% agar (agar-agar, Carl Roth). It was supplemented with 100 μg/mL Vancomycin (Duchefa Biochemie), unless other antibiotics were added as indicated below for transgene selection. During the first 7 days, protonemata were cultured on cellophane discs (AA Packaging) covering the medium surface to facilitate collection and transfer.[108]

For GFP imaging, qPCR analyses or preparation of extracts (protein co-purification assays, quantification of IAA content) protonemal cultures were grown on BCDA medium[109] (1 mM $MgSO_4$, 1.84 mM KH_2PO_4, 10 mM KNO_3, 5 mM ammonium-tartrate, 1 mM $CaCl_2$, 45 μM $FeSO_4$, 9.9 μM H_3BO_3, 2 μM $MnCl_2$, 116 nM $AlK(SO_4)_2$, 424 nM $CoCl_2$, 220 nM $CuSO_4$, 235 nM KBr, 168 nM KI, 660 nM LiCl, 124 nM $SnCl_2$ and 191 nM $ZnSO_4$) and were weekly sub-cultured after homogenization (Omni International) in millipore water. Every six weeks, fresh cultures were established from homogenized gametophores, which were collected from long-term cultures maintained on BCD medium (BCDA medium without NH_4-tartrate) at 15°C under white light illumination for 2 h per day with an intensity of 50 μmol m^{-2} s^{-1} (F17T8 cool white fluorescent tubes [17W], Phillips). Titratable expression of YFP and YFP fusion proteins was induced by supplementing the BCDA medium with β-estradiol (Sigma) dissolved in DMSO. Minimal estradiol concentrations required for expression levels detectable by fluorescence microscopy or Western Blotting were empirically determined for each analyzed line, varied between 1 and 10^{-5} μM and are listed in the key resources table (Experimental Models).

METHOD DETAILS

Protonemata regeneration from protoplasts

To analyze GUS expression, cell length, colony size, caulonema differentiation, the morphology of apical protonemal cells and colonies, or maximally induced estradiol-titratable Pp*RIC* overexpression, protoplasts were prepared from 1 week-old protonemal cultures based on treatment with 0.5% driselase (Sigma) as described.[28] After 2 days on PRMB medium (BCDA supplemented with 6% mannitol), which was solidified with 0.7% agar (high-strength agar, Merck), protonemata regenerating from isolated protoplasts were transferred to BCDA medium for the next 5 days, if not indicated otherwise. To investigate auxin effects on caulonema transition,

BCDA medium supplemented with 1 μM naphthalene acetic acid (NAA, Merck) dissolved in 50 mM NaOH (or with an equal volume of the solvent to prepare control samples) was used. BCDA medium was replaced by BCD or BCA (BCDA containing 10 mM KCl instead of KNO_3) medium to investigate effects of reduced nitrogen supply on caulonema differentiation. β-Estradiol (Sigma) at a concentration of 1 μM was added to BCDA medium to analyze effects of maximally induced estradiol-titratable Pp*RIC* overexpression. To determine the size of 5 weeks-old colonies and to analyze GUS expression in gametophores and sporophytes, regenerating protonemata were individually removed from cellophane discs after 5 days on BCDA medium and transferred to BCD plates.

Identification of RIC homologs, conserved sequences motives and NLSs

To identify plant and algal RIC and ROP homologs, full-length PpRIC, AtRIC1 and PpROP1 amino acid sequences and tBLASTn[96] were employed to search the following genome and transcriptome databases: TAIR (The Arabidopsis Information Resource),[98] NCBI (National Center for Biotechnology Information),[110] Phytozome (Joint Genome Institute),[101] ONEKP (China National GeneBank),[97] Gymno PLAZA (Ghent University),[100] and PhycoCosm (Joint Genome Institute).[102] URLs providing access to the databases searched and species represented in these databases are listed in Table S1, together with the accession numbers of identified RIC homologs and information concerning the presence of ROP homologs in all anal species. Species with high-quality genome databases were preferentially selected for display in Figure 1.

Identified RIC homologs were screened for conserved motifs using the MEME (Multiple Expectation Maximizations for Motif Elicitation)[95] tool (https://meme-suite.org/meme/tools/meme) with the following settings: maximally 1 occurrence of each motif per sequence, maximally 6 motives per sequence, and motif width 10 to 30 residues. The following motifs were identified, which are displayed in Figure 1 in the color indicated in brackets.

1) GWPPNYVARCPVTLFEAAGGSASWHNSGTV (light gray),
2) GELHMRPLGGAVJHFQLHDLLDGQVLFEHT (dark gray),
3) RFFVIRQENGSFRGFGFRDKDAAHEMKERI (gray),
4) MKRLJKGLKAJSQJFVWKE (light blue),
5) EMZIGYPTDVKHVAHIGWDGPSVNGP (CRIB domain, dark blue) and
6) WMDELRPAPDFSSAPLSDFGQPRGPDWIHD (blue).

The NLStradamus[103] tool (http://www.moseslab.csb.utoronto.ca/NLStradamus/) was employed to search identified RIC homologs for predicted NLSs (indicated in Figure 1 by circles or triangles).

Phylogenetic analysis of the *RIC* gene family

The amino acid sequences of all RIC homologs identified in the representative viridiplantae species displayed in Figure 1 were aligned in SeaView v4.7 using Clustal Omega.[104,105] Aligned amino acid sequences were subsequently reverted to nucleotide sequences and manually trimmed to roughly 285 bp long fragments (including gaps) coding for the CRIB domain and flanking regions (Table S3). Based on the alignment of these fragments, a maximum-likelihood phylogenetic tree was constructed in PhyML 3.0,[106] using the SMS function,[111] Bayesian Information Criterion, BIONJ starting trees, SPR tree improvement, 10 random start trees and the charophyte sequences as root. The best model obtained was HKY85 + G + I with the following characteristics: 1) estimated proportion of invariable sites: 0.062, 2) substitution rate categories: 4, 3) estimated transition/transversion ratio: 1.302, and 4) estimated gamma shape parameter: K 91, Llk −7971.35. Branch support was calculated using aBayes in PhyML 3.0. FigTree v1.4.3 was employed to display the tree as shown in Figure S1.

Knock-out, knock-in and expression constructs generated

Construction and analysis of recombinant plasmids was performed using standard methods[112,113] and *E. coli* DH5α. Phusion (New England Biolabs) or Verify (PCR-Biosystems) polymerases were employed to PCR amplify fragments to be cloned and plasmids to be mutagenized. PCR products and junctions between ligated fragments were verified by Sanger sequencing (Eurofins Genomics). All primers used and plasmids constructed are listed in Table S4 and in the key resources table (Recombinant DNA), respectively. Plasmids to be employed for stable *P. patens* transformation were constructed using the following vector backbones, which enable transgene integration based on homologous recombination into different neutral genomic regions (indicated in brackets): 1) pMP1180[88] (Pp108B[114]), 2) pTHUBI[85] (Pp108[114]), 3) pGX8[87] (PIG1b[115]), or 4) pCMAK1[86] (BS213[114]).

To knock-out Pp*RIC* based on homologous recombination (Pp*ric-1* mutant), the plasmid pSLU74 was generated by cloning 0.65 kb genomic Pp*RIC* fragments corresponding to regions upstream of bp −70 (start codon: bp 1) or downstream of bp 3205 (stop codon: bp 3101) into pMT123,[89] such that these fragments were flanking a plant expression cassette conferring hygromycin resistance[116] (Figure S2A). The plasmid introduced into a neutral region of the Pp*ric-1* genome to obtain complemented lines, which expressed PpRIC at essentially endogenous levels (Pp*ric-1*$^{comp-WT}$), was generated by cloning a 1700 bp genomic fragment corresponding to the Pp*RIC* promoter into the HindIII/AscI sites of pMP1180.[88] Into the AscI/PacI sites of the resulting plasmid, the Pp*RIC* cDNA was then inserted to generate pFAU342 (Pp*RIC*^{pro}:Pp*RIC*). To enable Pp*ric-1* complementation by introducing a *YFP*-Pp*RIC*^{gDNA} construct into the disrupted Pp*RIC* locus of this mutant based on homologous recombination, pFAU1211 (Figure S2A) was generated by simultaneously inserting using "In-Fusion Cloning" (Takara Bio Europe) the following five PCR products in the

indicated order into PCR-amplified linearized pMT164[90]: 1) a 0.65 kb genomic Pp*RIC* fragment corresponding to a region upstream of bp −70 (start codon: bp 1), 2) a *YFP* cDNA (without stop codon) amplified from pWEN240, 3) a genomic Pp*RIC* fragment comprising the complete coding region (all exons and introns) along with the 5′ end of the 3′ UTR, 4) a plant expression cassette conferring G418 resistance, and 5) a 0.65 kb genomic Pp*RIC* fragment corresponding to a region downstream of bp 3205 (stop codon: bp 3101). Care was taken to maintain the reading frame between the *YFP* cDNA and the Pp*RIC* coding region.

To knock-out Pp*RIC* based on CRISPR/Cas (Pp*ric-2 to -7* mutants), transient co-transformation with two plasmids was required.[84] pAct-Cas9 (Os*ACT*^{pro}:Sp*hCas9*[84]) needed to express Cas9 was obtained from Fabien Nogué (Université Paris-Saclay, Versailles, France). To generate the second plasmid, a DNA fragment (FAU-C475) was commercially synthesized (Eurofins Genomics), which contained between attB sites at both ends an expression cassette composed of the Pp*U6* promoter upstream of a region encoding a single guide RNA (sgRNA-Pp*RIC*). The 20 bp fragment in third Pp*RIC* exon (Figures S2A and S2E) to be targeted by this sgRNA was identified using CRISPOR.[99] Based on Gateway BP cloning,[117] the FAU-C475 fragment was inserted into pDONR207-KanR (Thermo Fisher Scientific) to generate pFAU709 (Pp*U6*^{pro}:sgRNA-Pp*RIC*, G418 resistance), or into pFAU832 (a pDONR207-KanR derivative) to create pFAU849 (Pp*U6*^{pro}:sgRNA-Pp*RIC*, hygromycin resistance).

To generate Pp*RIC*^{pro}:Pp*RIC*^{gDNA}-*GUS* reporter lines by knocking a *uidA* cDNA encoding GUS into the genomic Pp*RIC* locus based on homologous recombination, 0.6 kb genomic Pp*RIC* fragments upstream or downstream of the stop codon were cloned individually into pENTR/D-TOPO[117] to generate pSLU60 and pSLU61. After excision based on BamHI or NotI/XbaI restriction, respectively, the two fragments were sequentially cloned into pPpGUS[32] yielding pSLU62 (Figure S2A). To produce control reporter lines constitutively expressing GUS, the *uidA* cDNA amplified from pPpGUS was subcloned into pENTR/D resulting in pFAU182. Based on a Gateway LR reaction, the *uidA* cDNA was subsequently transferred into pTHUBI to create pFAU183 (Zm*UBQ*^{pro}:*GUS*).

To overexpress PpRIC, the Pp*RIC* cDNA was cloned in pENTR/D-TOPO generating pFAU166. Based on a Gateway LR reaction, the Pp*RIC* cDNA was then transferred into pTHUBI to generate pFAU168 (Zm*UBQ*^{pro}:Pp*RIC*), and into pGX8 resulting in pFAU820 (*est-ind*^{pro}:Pp*RIC*).

To enable estradiol-titratable YFP-PpRIC expression, the Pp*RIC* cDNA was inserted into NgomIV/SalI restricted pWEN240[93] downstream and in frame with a YFP cDNA[118] (eYFP, Clontech-Takara Bio Europe), resulting in pFAU366. The *YFP*-Pp*RIC* cDNA amplified from this plasmid was first cloned into pENTR/D-TOPO generating pFAU370, and subsequently transferred into pGX8 based on a Gateway LR reaction to create pFAU374 (*est-ind*^{pro}:*YFP*-Pp*RIC*$^{1\text{-}318aa}$). Based on the same cloning strategy the plasmids pFAU375 (*est-ind*^{pro}:*YFP*-Pp*RIC*$^{1\text{-}228aa}$), pFAU376 (*est-ind*^{pro}:*YFP*-Pp*RIC*$^{204\text{-}318aa}$) and pFAU377 (*est-ind*^{pro}:*YFP*-Pp*RIC*$^{204\text{-}228aa}$) were generated, which allow estradiol-titratable expression of YFP fused to truncated PpRIC. To enable estradiol-titratable YFP expression, the *YFP*-Pp*RIC* cDNA in pFAU374 was replaced by a *YFP* cDNA, which was amplified from pFAU374 and re-inserted into the NotI/AscI sites of the same plasmid, yielding pFAU702 (*est-ind*^{pro}:*YFP*).

To generate a nuclear marker construct, the Zm*UBQ*^{pro} promoter, a *PpH2B* cDNA and an *mCHERRY* cDNA[119] were PCR amplified from pFAU168, *P. patens* cDNA or pCAMBIA-mCHERRY,[91] respectively. All three fragments were then simultaneously introduced by "In-Fusion Cloning" (Takara Bio Europe) into NotI/EcoRI restricted pFAU168, resulting in pFAU733 (Zm*UBQ*^{pro}:Pp*H2B-mCHERRY*). A nucleolar marker construct was generated by PCR amplifying cDNAs encoding PpFIBRILLARIN (PpFIB) and mRFP from *P. patens* cDNA or pNCS-mRFP,[92] respectively, followed by "In-Fusion Cloning" (Takara Bio Europe) of both PCR fragments into XhoI/HpaI restricted pCMAK1 yielding pFAU740 (*35S*^{pro}:*mRFP*-Pp*FIB*).

To introduce point mutations into the two predicted PpRIC NLSs, entire plasmids were PCR amplified (1x: 98°C for 30 s, 18x: 98°C for 5 s -> 56°C for 10 s -> 72°C for 15 s/kb, 1 × 72°C for 5 min) using Phusion polymerase (New England Biolabs) and mutagenic primers, followed by DpnI restriction of methylated template DNA. To mutate NLS1 (K181A, K182A, R183A, R184A), pFAU374 was amplified using primers FAU-B197/FAU-B198 yielding pFAU420 (*est-ind*^{pro}:*YFP*-Pp*RIC* $^{\Delta NLS1}$). To mutate NLS2 (R313A), pFAU374 or pFAU420 were amplified using primers FAU-B766/FAU-B767 yielding pFAU500 (*est-ind*^{pro}:*YFP*-Pp*RIC* $^{\Delta NLS2}$) or pFAU505 (*est-ind*^{pro}:*YFP*-Pp*RIC* $^{\Delta NLS1\&2}$), respectively. The Pp*RIC* $^{\Delta NLS1\&2}$ cDNA PCR amplified from pFAU505 was introduced into PacI/AscI restricted pFAU342 to generate pFAU550 (Pp*RIC*^{pro}:Pp*RIC*$^{\Delta NLS1\&2}$), which enabled complementation analysis (Pp*ric-1*$^{comp-\ \Delta NLS1\&2}$).

To enable estradiol-titratable expression of YFP fused to isolated PpRIC NLSs, a YFP cDNA was amplified from FAU374 using a reverse primer containing an NLS1 anti-sense sequence at the 5′ end. The resulting *YFP-NLS1* PCR fragment was introduced into NotI/AscI restricted pFAU374 to generate pFAU747 (*est-ind*^{pro}:*YFP-NLS1*). Furthermore, cDNAs encoding YFP and NLS2 were individually amplified from FAU374 followed by "In-Fusion Cloning" (Takara Bio Europe) of both PCR products into NotI/AscI restricted pFAU374, yielding pFAU493 (*est-ind*^{pro}:*YFP-NLS2*).

To generate a construct allowing the purification of a recombinant GST-PpROP1^{Q64L} fusion protein from *E. coli*, the Pp*ROP1* cDNA was amplified from *P. patens* cDNA and inserted into XmaI/NotI restricted pGEX4T2 (VWR) to create pFAU311. pFAU311 was amplified using mutagenic primers FAU-596/FAU-597 followed by DpnI restriction of template DNA (see mutagenesis of PpRIC NLSs) to generate pFAU312 (*tac*^{pro}:*GST*-Pp*ROP1*^{Q64L}), which contains a bacterial GST-PpROP1^{Q64L} expression cassette.

Expression constructs and *P. patens* lines obtained

A plasmid with a Gm*GH3*^{pro}:*GUS* expression cassette (pRTGH3:GUS[66]), which was obtained from Ralf Reski (University of Freiburg, Germany) and does not contain homologues sequences enabling transgene integration into neutral genomic regions, was introduced into wild type *P. patens* to generate transgenic auxin response reporter lines. To knock-out Pp*RIC* in this transgenic background

based on CRISPR/Cas, pAct-Cas9[84] provided by Fabien Nogué (Université Paris-Saclay, Versailles, France) and pFAU849 were employed. A plasmid containing a Pp*PINA*^{prom}:Pp*PINA-swGFP* cassette conferring expression of eGFP[120] sandwich-tagged PpPINA (PpPIN$^{1\text{-}552}$-eGFP-PpPIN$^{553\text{-}713}$) under the control of the endogenous Pp*PINA* promoter[33] was obtained from Mattias Thelander (Swedish University of Agricultural Sciences, Uppsala). This plasmid was used to introduce the Pp*PINA*^{prom}:Pp*PINA-swGFP* cassette into the neutral genomic region P108[114] of wild type as well as Pp*ric-1* plants. Mattias Thelander also provided Pp*pina/b*[33] and Pp*shi1*[32] knock-out mutants as well as a transgenic Pp*SHI1*^{OEX} overexpression line.[32]

Protoplast transformation and CRISPR/Cas mutagenesis

Knock-out, knock-in or expression constructs were introduced into *P. patens* protoplasts by PEG-mediated transformation as described,[28] based on a previously established protocol.[109] Transgenic lines were selected on antibiotics (30 μg/mL hygromycin B [Carl Roth], 20 μg/mL G418 [Merck], and/or 50 μg/mL Zeocin [Thermo Fisher Scientific]), depending on the construct used (key resources table; Recombinant DNA). For CRISPR/Cas mutagenesis using the approach developed by Collonnier and coworkers,[84] essentially the same protoplast transformation procedure was employed with the following modifications: 1) circular instead linearized plasmid DNA (pAct-Cas9 and pFAU709 or pFAU849) was used, and 2) after 4 days on PRMB medium, regenerating protonemata were kept for 4 days on BCDA medium containing antibiotics as required (20 μg/mL G418 or 30 μg/mL hygromycin B), before they were transferred to antibiotic-free BCDA medium.

PCR genotyping of transgenic and mutant lines

All transgenic and/or mutant *P. patens* lines generated in this study are listed in the key resources table (Experimental models). To PCR genotype these lines, genomic DNA was isolated from 4 to 7-days old protonemata according to Cove and coworkers[109] with some modifications.[28] The Optima polymerase (Nippon Genetics) and primers listed in Table S4 were employed to amplify genomic fragments characteristic for each line, which were confirmed by sequencing (Eurofins Genomics). Genotyping of PpRIC-GUS reporter lines, of the Pp*ric-1* mutant, and of complemented Pp*ric-1*$^{comp-YFP-WT}$ lines, which were generated based on homologous recombination, is displayed in Figure S2B. To identify indels at the sgRNA target site in Pp*ric* knock-out mutants generated based on CRISPR/Cas (Figures S2E and S2F), genomic fragments spanning this target site were amplified using primers FAU-C123/FAU-B757 (Figure S2A) and sequenced. In addition, to confirm loss of the CAS9 expression cassette in CRISPR/Cas knock-out mutants after transfer to antibiotic-free BCDA medium, PCR reactions using primers FAU-C562/FAU-C563 were performed. With the exception of lines constitutively expressing PpH2B-mCHERRY or mRFP-PpFIBRILLARIN markers, which were selected based on fluorescence emission, and of lines containing randomly inserted Gm*GH3*^{pro}:*GUS* expression cassettes, all other transgenic lines were genotyped by PCR amplifying characteristic genomic fragments spanning the insertion sites at the 5′ AND-3′ ends of transgenes using primers listed in Table S4.

qRT-PCR expression analysis

Extracts prepared from 4 to 7-days old protonemata, from gametophores or from sporophytes using a TissueLyser II (Qiagen), and the Nucleospin RNA Plus Kit (Macherey-Nagel), were employed to prepare total RNA, which was subjected to agarose gel electrophoresis for quality control. cDNA reverse transcribed from 500 ng total RNA using the iScript cDNA Synthesis Kit (BioRad), the SYBR Green Master Mix (BioRad) and a CFX96TM thermal cycler (BioRad) were employed for qRT-PCR analysis. Pp*UBIQUITIN-E2* served as reference gene.[121] To determine absolute transcript levels, standard curves were established based on 10-fold serial dilution of genomic DNA extracted from 4 to 7-days old protonemata using the PhytoPure DNA Extraction kit (Cytiva). Relative transcript levels were determined according to the $2^{-\Delta\Delta Ct}$ method using the value obtained for one reference replicate as calibrator (relative expression = 1). In each experiment, three biological replicates and two or three technical replicates per sample were analyzed. All experiments were repeated at least twice. PCR primers used are listed in Table S4.

Histochemical GUS expression analysis

Cellophane discs were transferred 1 to 5 days after protoplast preparation and plating to fresh Petri dishes containing 4 mL GUS staining solution (100 mM Na_2PO_4 buffer, pH 7.0, 5 mM $K_3[Fe(CN)_6]$, 5 mM $K_4[Fe(CN)_6]$, 0.1% Triton X-100, 4 mM 5-Bromo-4-chloro-3-indolyl-β-D-glucuronic acid) and incubated overnight at 37°C. Digital bright field images were acquired using a wide-field microscope (DMI4000B, Leica) or a stereo microscope (M205FA, Leica).

Analysis of caulonema differentiation, cell length and colony size

Digital bright field images of 5 days-old protonemata regenerating from protoplasts were recorded using a wide-field microscope (DMI4000B, Leica) to analyze cell-length and caulonema differentiation. Fiji software (ImageJ 1.53c[94]) was employed to measure the length of subapical chloronemal or caulonemal cells. The percentage of protonemal filaments with apical cells displaying caulonemal characteristics was determined by optical inspection. Only filaments composed of at least 3 cells were taken into account for this analysis. Digital images recorded using an epi-fluorescence stereo microscope (M205FA, Leica) and Fiji software were employed to measure the size of 5 days-old protonemata or 5 weeks-old colonies. The area covered by 5 days-old protonemata was determined based on chlorophyll autofluorescence images (excitation 470 nm, emission: 500 nm long-pass) using a Fiji macro described in the literature.[122] To determine the area of 5 weeks-old colonies, thresholding was applied to convert reflected light 8-bit images to 1-bit.

Confocal microscopy and quantitative analysis of nuclear targeting

Confocal imaging was performed using a Leica TCS SP8 DIVE-FALCON inverted laser scanning confocal microscope, which was run by Application Suite X software and equipped with an HC PL APO CS2 20X/0.75 NA water immersion lens. Along with each confocal image of fluorescent protein distribution, a transmitted-light reference image (Nomarski) and a confocal image showing chloroplast autofluorescence were simultaneously recorded. An Argon laser was employed to excite GFP (488 nm), YFP (514 nm) and chlorophyll (514 nm). mCHERRY and mRFP were excited using a 561 nm DPSS laser. Fluorescence emitted by different fluorophores was imaged using the following wave length windows: 500–550 nm (GFP), 524–547 nm (YFP), 566–600 nm (mCHERRY), 566–623 nm (mRFP), and 669–745 nm (chlorophyll).

To quantitatively analyze nuclear targeting of YFP or YFP fusion proteins in subapical cells of 4–7 days old protonemata, Z-stacks of confocal optical sections were recorded at a step size of 2 μm. Fiji software was employed to generate single plane projections of these Z-stacks, to subtract background signal recorded next to imaged cells and to determine integrated fluorescence intensities. Cellular, nuclear and nucleolar borders were manually outlined in the analyzed projections. Occasionally, nucleoli labeled by YFP-PpRIC fusion proteins were not sharply delimited. The borders of these nucleoli were manually outlined such that they enclosed an average area cross section. Projections with manually outlined compartmental borders were used to determine the integrated fluorescence intensity of 1) each imaged whole cell (cytoplasm and nucleus), 2) the whole nucleus within each cell (nucleoplasm and nucleolus) and 3) the nucleolus within each nucleus.

Determination of free IAA content

Extracts of 7-days old protonemata (around 15–30 mg fresh weight per sample) were supplemented with 500 pg ^{13}C6-IAA internal standard per sample and analyzed in triplicates for free IAA content using combined gas chromatography-tandem mass spectrometry as described.[123]

YFP-PpRIC co-purification with GST-PpROP1^{Q64L}

GST or GST-PpROP1^{Q64L} expression in *E. coli* BL21(DE3) transformed with pGEX4T2 (VWR) or pFAU312 (*tac^{pro}:GST-PpROP1^{Q64L}*), respectively, was induced for 2.5 h at 37°C in the presence of 0.1 mM Isopropyl-β-D-thiogalactopyranoside. To prepare extracts, cells were 1) collected by centrifugation, 2) resuspended in IPP100 buffer (10 mM Tris-HCl, pH 7.3, 100 mM NaCl, 0.1% NP40) containing 1 mg/mL lysozyme and Complete protease inhibitor mix (Merck), and 3) lysed by sonication (UW2070, Bandelin; 3 × 20 s, 70% output). After debris removal by centrifugation, total protein content of soluble cell extract was determined by Bradford assay (Merck). Equal volumes (750 μL) of soluble extract containing 20 to 100 μg total protein were supplemented with 20 μL MagneGST beads (Promega) and rotated at 4°C for 1 h. GST-PpROP1^{Q64L}-loaded MagneGST beads were collected by magnetic separation, washed with IPP100 buffer containing Complete protease inhibitor mix (Merck) and immediately used for YFP-PpRIC co-purification assays.

Estradiol-titratable expression of full length or truncated YFP-PpRIC fusion proteins was induced by transferring 4 to 6 days-old transgenic protonemata onto BCDA medium containing 1 μM β-estradiol for 16 h. After induction, protonemata (200 mg fresh weight) were collected, dried with filter paper (Whatman), frozen in liquid nitrogen, ground in a mortar with a pestle, and extracted in 200 μL of RIPA buffer (10 mM Tris-HCl, pH 7.5, 150 mM NaCl, 0.5 mM EDTA, 1% Triton X-, 1% deoxycholate) supplemented with Complete protease inhibitor mix (Merck). Soluble fractions obtained by extract centrifugation were supplemented with 300 μL dilution buffer (10 mM Tris-HCl buffer, pH 7.5, 150 mM NaCl, 0.5 mM EDTA) containing Complete protease inhibitor mix (Merck). After determination of protein content by Bradford assay (Merck), different volumes of soluble fractions containing equal amounts of total protein were added to PpROP1^{Q64L}-loaded MagneGST beads. After 1h rotation at 4°C, beads were collected by magnetic separation, washed with dilution buffer and boiled in 3xSDS-loading buffer. After PAGE (polyacrylamide gel electrophoresis) separation, bead-associated proteins were detected by immunoblotting using primary monoclonal mouse anti-GST (G1160, Merck; 1:2000) or polyclonal rabbit anti-GFP (G1544, Merck; 1:4000) antibodies, and secondary HRP (horseradish peroxidase) conjugated anti-mouse IgG (W4028, Promega; 1:15,000) or anti-rabbit IgG (W4018, Promega; 1:1000) antibodies.

QUANTIFICATION AND STATISTICAL ANALYSIS

Statistical significance of differences between samples was assessed using unpaired Student's t Test (two samples), Welch's ANOVA or ANOVA followed by Tukey's multiple comparison test (three or more samples) as indicated in the figure legends. Pairwise comparisons essential for data interpretation are indicated in graphs and figures (all others are listed in Table S2). All statistical analyses were performed using GraphPad Prism (Version 9.3.1, GraphPad software).